



Cold-water corals in the Subpolar North Atlantic Ocean exposed to aragonite undersaturation if the 2 °C global warming target is not met

Maribel I. García-Ibáñez^{a,b,*}, Nicholas R. Bates^{c,d}, Dorothee C.E. Bakker^a, Marcos Fontela^{b,e}, Antón Velo^b

^a Centre for Ocean and Atmospheric Sciences, School of Environmental Sciences, University of East Anglia, Norwich, United Kingdom

^b Instituto de Investigaciones Marinas, CSIC, Eduardo Cabello 6, 36208 Vigo, Spain

^c Bermuda Institute of Ocean Sciences (BIOS), 17 Biological Lane, St. Georges, Bermuda

^d Department of Ocean and Earth Science, University of Southampton, Southampton, UK

^e Center of Marine Sciences (CCMAR), Universidade do Algarve, 8005-139 Faro, Portugal

ARTICLE INFO

Keywords:

Ocean acidification
Aragonite saturation state
Atlantic Meridional Overturning Circulation
Eastern-Subpolar North Atlantic Ocean

ABSTRACT

The net uptake of carbon dioxide (CO₂) from the atmosphere is changing the ocean's chemical state. Such changes, commonly known as ocean acidification, include a reduction in pH and the carbonate ion concentration ([CO₃²⁻]), which in turn lowers oceanic saturation states (Ω) for calcium carbonate (CaCO₃) minerals. The Ω values for aragonite (Ω_{aragonite}; one of the main CaCO₃ minerals formed by marine calcifying organisms) influence the calcification rate and geographic distribution of cold-water corals (CWCs), important for biodiversity. Here, high-quality measurements, collected on thirteen cruises along the same track during 1991–2018, are used to determine the long-term changes in Ω_{aragonite} in the Irminger and Iceland Basins of the North Atlantic Ocean, providing the first trends of Ω_{aragonite} in the deep waters of these basins. The entire water column of both basins showed significant negative Ω_{aragonite} trends between -0.0014 ± 0.0002 and -0.0052 ± 0.0007 per year. The decrease in Ω_{aragonite} in the intermediate waters, where nearly half of the CWC reefs of the study region are located, caused the Ω_{aragonite} isolines to rapidly migrate upwards at a rate between 6 and 34 m per year. The main driver of the decline in Ω_{aragonite} in the Irminger and Iceland Basins was the increase in anthropogenic CO₂. But this was partially offset by increases in salinity (in Subpolar Mode Water), enhanced ventilation (in upper Labrador Sea Water), and increases in alkalinity (in classical Labrador Sea Water, cLSW; and overflow waters). We also found that water mass aging reinforced the Ω_{aragonite} decrease in cLSW. Based on these Ω_{aragonite} trends over the last three decades, we project that the entire water column of the Irminger and Iceland Basins will likely be undersaturated for aragonite when in equilibrium with an atmospheric mole fraction of CO₂ (xCO₂) of ~880 ppmv, corresponding to climate model projections for the end of the century based on the highest CO₂ emission scenarios. However, intermediate waters will likely be aragonite undersaturated when in equilibrium with an atmospheric xCO₂ exceeding ~630 ppmv, an xCO₂ level slightly above that corresponding to 2 °C global warming, thus exposing CWCs inhabiting the intermediate waters to undersaturation for aragonite.

1. Introduction

The global ocean has absorbed ~30% of the anthropogenic CO₂ (i.e., C_{ant}; CO₂ from human activities) released into the atmosphere since the industrial revolution (Friedlingstein et al., 2019; Gruber et al., 2019) and will likely sequester ~85% of C_{ant} emissions on the time scales of several thousands of years (Archer et al., 2009). The global oceanic C_{ant} uptake has mitigated atmospheric CO₂ concentration increases due to

C_{ant} emissions, and thereby climate change, but has also resulted in an unprecedented rapid long-term shift in the ocean's chemical state known as ocean acidification (OA; e.g., Raven et al., 2005; Gattuso et al., 2014; Williamson and Widdicombe, 2018; Doney et al., 2020). OA refers to the reduction in oceanic pH caused primarily by uptake of atmospheric CO₂ (IPCC, 2011), which in turn reduces the carbonate ion concentration ([CO₃²⁻]) and the ocean's capacity to take up CO₂ (i.e., oceanic buffer capacity or Revelle factor; Bates et al., 2014). Such

* Corresponding author at: Centre for Ocean and Atmospheric Sciences, School of Environmental Sciences, University of East Anglia, Norwich, United Kingdom.
E-mail addresses: m.garcia-ibanez@uea.ac.uk (M.I. García-Ibáñez), nick.bates@bios.edu (N.R. Bates), d.bakker@uea.ac.uk (D.C.E. Bakker), mmfontela@ualg.pt (M. Fontela), avelo@iim.csic.es (A. Velo).

<https://doi.org/10.1016/j.gloplacha.2021.103480>

Received 16 November 2020; Received in revised form 15 March 2021; Accepted 29 March 2021

Available online 2 April 2021

0921-8181/© 2021 The Authors. Published by Elsevier B.V. This is an open access article under the CC BY license (<http://creativecommons.org/licenses/by/4.0/>).

changes in ocean chemistry may have direct and indirect consequences for marine life and ecosystems (particularly calcifying organisms; e.g., Riebesell et al., 2000; Kroeker et al., 2013; Pörtner et al., 2014; Mostofa et al., 2016; Doney et al., 2020).

A key parameter for understanding how changes in $[\text{CO}_3^{2-}]$ affect marine calcifying organisms is the seawater saturation state for calcium carbonate (CaCO_3) minerals (i.e., Ω ; Eq. 1):

$$\Omega = [\text{Ca}^{2+}] \cdot [\text{CO}_3^{2-}] / K_{sp}' \quad (1)$$

where Ω is defined as the ratio between the product of the in situ concentrations of calcium ions ($[\text{Ca}^{2+}]$) and $[\text{CO}_3^{2-}]$ and their expected concentrations when the solution is in equilibrium with a particular CaCO_3 mineral phase such as calcite (Ω_{calcite}) or aragonite ($\Omega_{\text{aragonite}}$) parameterized through the apparent solubility product (K_{sp}'). Seawater is in equilibrium with a particular CaCO_3 mineral phase when $\Omega = 1$, supersaturated when $\Omega > 1$, and undersaturated when $\Omega < 1$ (e.g., Zeebe and Wolf-Gladrow, 2001). Since variability in $[\text{Ca}^{2+}]$ in the open ocean is relatively small and very closely related to variations in salinity (Riley and Tongudai, 1967; Millero, 1995), Ω is primarily controlled by $[\text{CO}_3^{2-}]$ and K_{sp}' . The Ω is lower in the deep ocean than in the upper ocean due to the dependence of K_{sp}' on pressure and to a lesser extent on temperature, in combination with the total dissolved inorganic carbon (DIC) build-up from the remineralization of organic matter and the temperature effects on the CO_2 equilibrium constants. This fact, combined with the high $[\text{CO}_3^{2-}]$ of the upper ocean due to its higher pH, leads to generally supersaturated surface waters and undersaturated deep waters. Below the saturation horizon ($\Omega = 1$), CaCO_3 becomes thermodynamically unstable and tends to dissolve. However, CaCO_3 can dissolve even though $\Omega > 1$ due to biologically-mediated processes (Milliman et al., 1999).

Cold-water coral (CWC) reefs are biodiversity hotspots, with the highest diversity occurring at 200–1000 m depth (Roberts et al., 2009). Aragonite is the main CaCO_3 mineral in CWC skeletons, for species such as *Lophelia pertusa* or *Madrepora oculata* (Roberts et al., 2009). The geographic distribution of CWCs, with over 95% of all presently known reefs located above the aragonite saturation horizon (ASH; $\Omega_{\text{aragonite}} =$

1) in preindustrial times, suggests that waters supersaturated for aragonite may be critical for their existence (Guinotte et al., 2006). In the North Atlantic Ocean, the Atlantic Meridional Overturning Circulation (AMOC) with deep-water formation in the Greenland, Iceland, Norwegian, and Labrador Seas causes the ASH to be the deepest in the global ocean at more than 2000 m depth (e.g., Feely et al., 2004; Jiang et al., 2015). A chemically-favorable deep-water environment allows a broad distribution of CWC communities in the North Atlantic Ocean (Fig. 1; Guinotte et al., 2006; Tittensor et al., 2010). A corollary is that the AMOC drives a large deep-water penetration of C_{ant} in the North Atlantic Ocean (Sabine et al., 2004; Khatiwala et al., 2013; DeVries, 2014), leading to a substantial shoaling of the ASH by 80–400 m since preindustrial times (Wallace, 2001; Alvarez et al., 2003; Feely et al., 2004; Tanhua et al., 2007; Pérez et al., 2013, 2018). By the end of the century, further uptake of C_{ant} is projected to shoal the North Atlantic Ocean ASH depth by more than 2000 m under the IS92a ‘business-as-usual’ scenario (Orr et al., 2005) and reduce the pH by more than 0.2 units over 21% of the seafloor area below 500 m depth in the North Atlantic sector based on RCP8.5 (Gehlen et al., 2014). Such shoaling of the ASH and pH reduction will alter the chemical environment of intermediate and deep waters and expose the majority of the CWC reefs to undersaturated (potentially corrosive) waters for aragonite. Therefore, CWC biomes are predicted to be one of the first deep marine ecosystems affected by OA (Raven et al., 2005; Guinotte et al., 2006; Turley et al., 2007; Maier et al., 2009; Roberts et al., 2009).

Previous studies have focused on the changes in $\Omega_{\text{aragonite}}$ at local and global scales (e.g., Feely et al., 2004; Orr et al., 2005; Jiang et al., 2015), and the possible environmental drivers of these changes (e.g., Murata et al., 2015; Omar et al., 2016; Turi et al., 2016; Xu et al., 2020). However, none of them focused on changes in $\Omega_{\text{aragonite}}$ and their drivers in the Irminger and Iceland Basins in the Subpolar North Atlantic Ocean (Fig. 1). The Subpolar North Atlantic Ocean may serve as a ‘natural laboratory’ of the effect of OA on deep-water benthic ecosystems (Andersson et al., 2011) for all the reasons aforementioned (e.g., CWC biomes, substantial C_{ant} uptake and deep-water penetration of C_{ant} , and possible changes in the AMOC system).

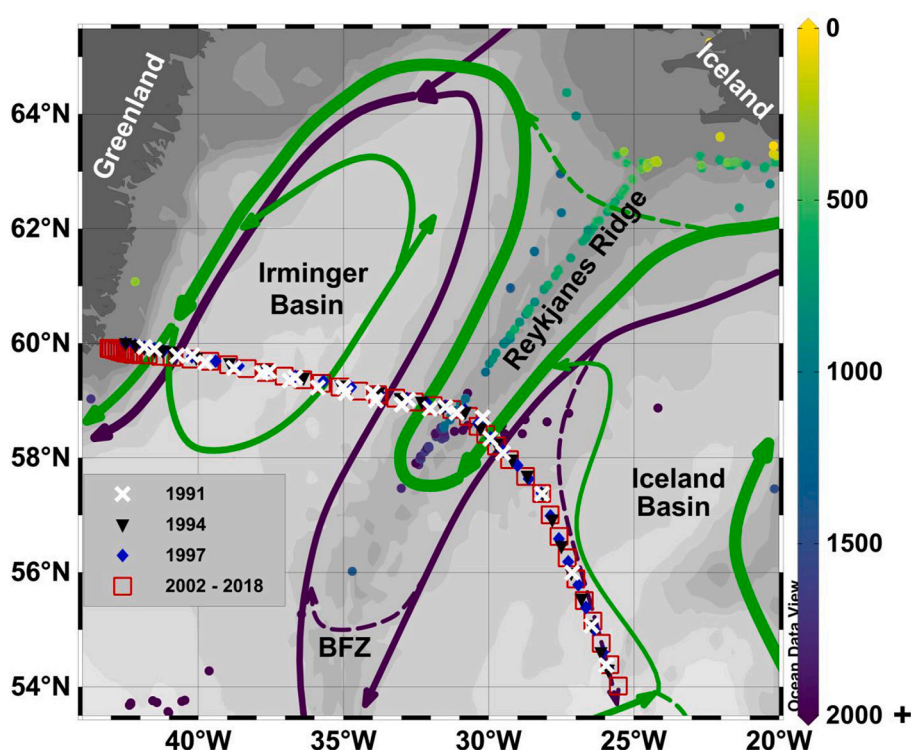


Fig. 1. Schematic circulation of the upper (green) and lower (dark purple) limbs of the Atlantic Meridional Overturning Circulation in the study region, adapted from Danialt et al. (2016). White crosses, black triangles, blue diamonds, and red squares represent station locations across the Irminger and Iceland Basins (list of cruises in Table S1). Colored dots represent known cold-water coral reefs (Freiwald et al., 2017), where the colour represents their depth (colour scale; in m). BFZ stands for Bight Fracture Zone. Figure produced with Ocean Data View (Schlitzer, 2020). (For interpretation of the references to colour in this figure legend, the reader is referred to the web version of this article.)

In this work, we describe long-term $\Omega_{\text{aragonite}}$ trends in the entire water column of the Irminger and Iceland Basins during 1991–2018, using high-quality oceanic observations of the seawater CO_2 -carbonate system variables collected during thirteen cruises, providing the first published trends of $\Omega_{\text{aragonite}}$ in the deep waters of the Irminger and Iceland Basins. García-Ibáñez et al. (2016) reported the observed reduction in pH and its drivers in the main water masses of these basins for 1991–2015. This work builds on that study by examining the consequences of the pH reduction on $\Omega_{\text{aragonite}}$ and the physical and chemical drivers of the $\Omega_{\text{aragonite}}$ changes, such as freshwater impacts and biogeochemical and transport/mixing impacts. We discuss our estimated $\Omega_{\text{aragonite}}$ trends in the context of previously reported trends. Finally, we use the observed $\Omega_{\text{aragonite}}$ trends to estimate the expected changes in $\Omega_{\text{aragonite}}$ for future increases in atmospheric CO_2 . Those projections are used to infer when deep CWC communities inhabiting the Subpolar North Atlantic Ocean would be exposed to waters undersaturated for aragonite.

2. Datasets and methodology

2.1. Dataset

Thirteen cruises along the same track across the Irminger and Iceland Basins were selected for our synthesis of the $\Omega_{\text{aragonite}}$ temporal evolution, spanning 28 years from 1991 to 2018 (Fig. 1; Table S1). Earlier data were extracted from the GLODAPv2.2020 data product, which provides bias-corrected, cruise-based, interior ocean data (Key et al., 2015; Olsen et al., 2020). This historical data was supplemented by hydrographic and seawater CO_2 chemistry data collected during the OVIDE 2018 cruise (Lherminier, 2018).

The accuracy of the GLODAPv2 data product is better than 0.005 for salinity, 2% for inorganic nutrients, $4 \mu\text{mol kg}^{-1}$ for DIC and total alkalinity (TA), and 0.01 for pH (Olsen et al., 2020). For the OVIDE cruise in 2018, the overall accuracy of nutrients was 1%, $2 \mu\text{mol kg}^{-1}$ for TA, and 0.0014 for pH.

For cruises with DIC measurements only, TA was computed according to Velo et al. (2013) procedures, using temperature, salinity, nitrate, phosphate, silicate, and oxygen as predictor parameters. The uncertainty of climatological TA is $5.4 \mu\text{mol kg}^{-1}$ (Velo et al., 2013).

For cruises with TA and pH measurements, DIC was computed from TA and pH. These calculated DIC values have an associated average uncertainty of $6.3 \mu\text{mol kg}^{-1}$, calculated with the CO2SYS errors program (Orr et al., 2018), taking into account the uncertainties in the input variables and the default errors for carbonate and borate system constants. $\Omega_{\text{aragonite}}$ was calculated (at in situ temperature and pressure) from temperature, salinity, DIC, and TA data (plus inorganic nutrients data). The uncertainty in calculated $\Omega_{\text{aragonite}}$ was 0.077 on average computed with the CO2SYS errors program (Orr et al., 2018) and default errors for carbonate and borate system constants and the uncertainties in the input variables. In particular, uncertainty in calculated $\Omega_{\text{aragonite}}$ was 0.078 for cruises with measurements of DIC and climatological TA, and 0.077 for cruises with measurements of TA and DIC estimated from TA and pH.

All calculations for the carbonate system were conducted using CO2SYS (Lewis and Wallace, 1998) for MATLAB (van Heuven et al., 2011), with the carbonic acid dissociation constants of Mehrbach et al. (1973) as reformulated on the total hydrogen scale by Lueker et al. (2000), the bisulfate dissociation constant of Dickson (1990), and the borate-to-salinity ratio of Uppström (1974).

2.2. Trend determination

The temporal changes in $\Omega_{\text{aragonite}}$ and their potential drivers were determined in the main water-mass layers in the Irminger and Iceland Basins, namely Subpolar Mode Water (SPMW), upper and classical Labrador Sea Water (uLSW and cLSW, respectively), Iceland–Scotland

Overflow Water (ISOW) and Denmark Strait Overflow Water (DSOW) (Fig. 2a).

Trends in $\Omega_{\text{aragonite}}$ and their drivers were calculated using the area-weighted average values of interpolated bottle data at dbar resolution while considering the thickness of the layer and the distance between measurements (García-Ibáñez et al., 2016). For $\Omega_{\text{aragonite}}$, a pressure-dependent variable (e.g., Dickson et al., 2007), a single reference pressure per water-mass layer (Table 1) was defined to remove pressure effects due to varying sampling strategies.

To determine the causes of the temporal changes in $\Omega_{\text{aragonite}}$, we assumed linearity to decompose the $\Omega_{\text{aragonite}}$ change into that associated with each of the potential drivers, using a first-order Taylor-series deconvolution (Kwiatkowski and Orr, 2018):

$$\Delta\Omega = \sum \frac{\partial\Omega}{\partial\text{Driver}} \frac{d\text{Driver}}{dt} = \frac{\partial\Omega}{\partial T}\Delta T + \frac{\partial\Omega}{\partial S}\Delta S + \frac{\partial\Omega}{\partial TA}\Delta TA + \frac{\partial\Omega}{\partial DIC}\Delta DIC \quad (2)$$

where $\Delta\Omega$ is the temporal change in $\Omega_{\text{aragonite}}$ while ΔT , ΔS , ΔTA , and ΔDIC are the corresponding temporal changes in in situ temperature (T), salinity (S), TA, and DIC.

We separated the freshwater impacts on DIC and TA from the changes related to variations in ocean internal biogeochemical processes and transport/mixing (e.g., Keeling et al., 2004; Lovenduski et al., 2007; Hauri et al., 2013):

$$\Delta\Omega = \frac{\partial\Omega}{\partial T}\Delta T + \frac{\partial\Omega}{\partial S}\Delta S + \frac{\overline{sTA}}{S_0} \frac{\partial\Omega}{\partial TA}\Delta S + \frac{\overline{s}}{S_0} \frac{\partial\Omega}{\partial TA}\Delta sTA + \frac{\overline{sDIC}}{S_0} \frac{\partial\Omega}{\partial DIC}\Delta S + \frac{\overline{s}}{S_0} \frac{\partial\Omega}{\partial DIC}\Delta sDIC \quad (3)$$

where S_0 is the reference salinity, which is set to 35 (Normal Standard Seawater; Millero et al., 2008; very close to the average salinity observed in our dataset, $S = 34.94$). $sDIC$ and sTA are the DIC and TA values normalized to a salinity of 35 and assuming a non-zero freshwater end-member (Friis et al., 2003). \overline{sTA} , \overline{s} , and \overline{sDIC} correspond to the average values of sTA , S , and DIC during 1991–2018. Regrouping the terms related to the contribution from freshwater forcing on $\Omega_{\text{aragonite}}$ gives the following equation:

$$\Delta\Omega = \frac{\partial\Omega}{\partial T}\Delta T + \left(\frac{\partial\Omega}{\partial S} + \frac{\overline{sTA}}{S_0} \frac{\partial\Omega}{\partial TA} + \frac{\overline{sDIC}}{S_0} \frac{\partial\Omega}{\partial DIC} \right) \Delta S + \frac{\overline{s}}{S_0} \frac{\partial\Omega}{\partial TA} \Delta sTA + \frac{\overline{s}}{S_0} \frac{\partial\Omega}{\partial DIC} \Delta sDIC \quad (4)$$

We separated $\Delta sDIC$ into C_{ant} and natural DIC (C_{nat}):

$$\Delta\Omega = \frac{\partial\Omega}{\partial T}\Delta T + \left(\frac{\partial\Omega}{\partial S} + \frac{\overline{sTA}}{S_0} \frac{\partial\Omega}{\partial TA} + \frac{\overline{sDIC}}{S_0} \frac{\partial\Omega}{\partial DIC} \right) \Delta S + \frac{\overline{s}}{S_0} \frac{\partial\Omega}{\partial TA} \Delta sTA + \frac{\overline{s}}{S_0} \frac{\partial\Omega}{\partial DIC} (\Delta sC_{\text{nat}} + \Delta sC_{\text{ant}}) = \Delta\Omega_T + \Delta\Omega_S + \Delta\Omega_{sTA} + \Delta\Omega_{sDIC} \quad (5)$$

The sensitivity of $\Omega_{\text{aragonite}}$ to each driver ($\frac{\partial\Omega}{\partial\text{driver}}$) was estimated by allowing a change in only one driver according to their observed trend while setting the other drivers to their average value during 1991–2018.

C_{nat} values were determined as the difference between DIC and C_{ant} , with C_{ant} values determined through the back-calculation technique φC_T^0 (Vázquez-Rodríguez et al., 2009; Vázquez-Rodríguez et al., 2012; Ríos et al., 2012). This latter method has been used to describe C_{ant} variability along the Atlantic Ocean and reported estimates were in agreement with those determined with other carbon-based and chlorofluorocarbon-based methods (Vázquez-Rodríguez et al., 2009; Fajar et al., 2015; Guallart et al., 2015; Fröb et al., 2018). Overall, the uncertainty of φC_T^0 -derived C_{ant} has been reported to be $5 \mu\text{mol kg}^{-1}$ (Pérez et al., 2008; Vázquez-Rodríguez et al., 2009).

The temporal trends in $\Omega_{\text{aragonite}}$ and their drivers were calculated considering the variability within each layer using a weighted simple linear regression analysis, where the weights were assigned as the

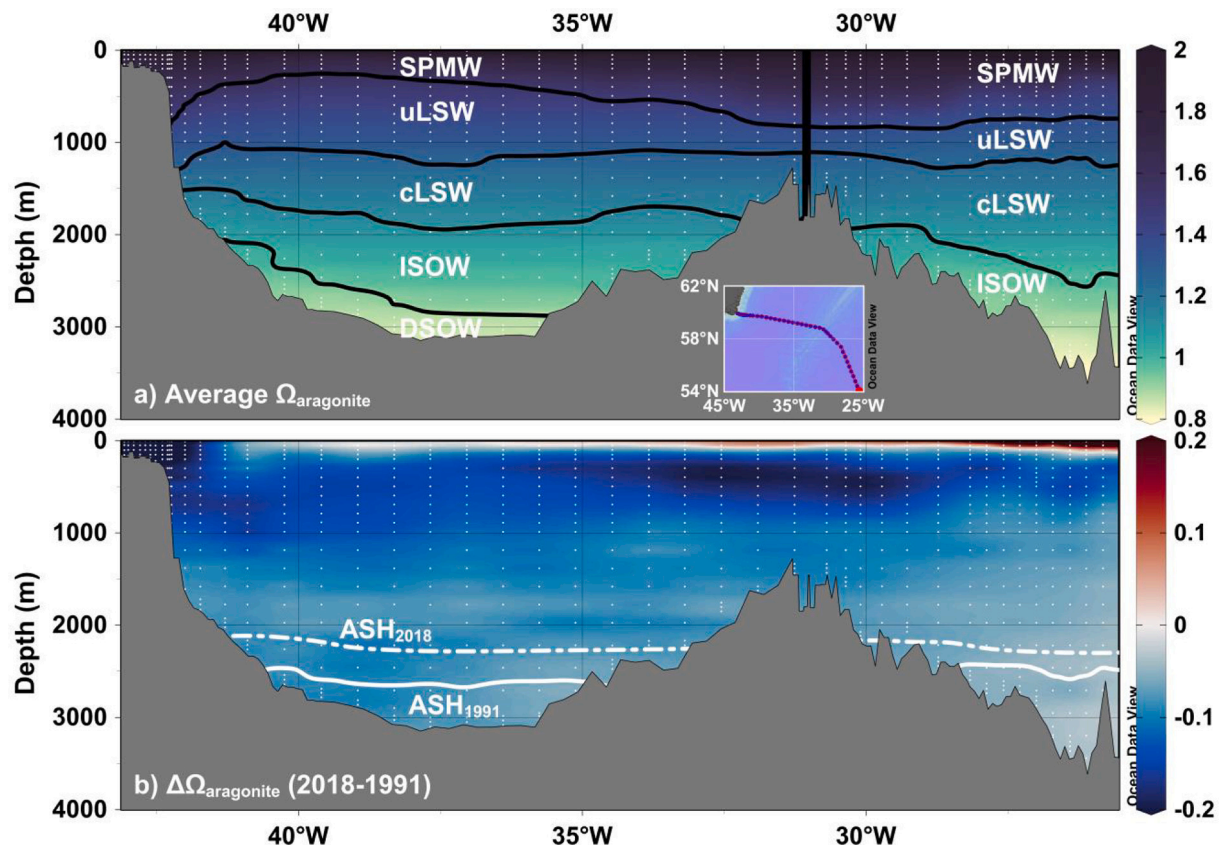


Fig. 2. (a) Average aragonite saturation state ($\Omega_{\text{aragonite}}$) along the section (inset) during 1991–2018. Black lines depict the limits of basins and water-mass layers (Table 1). (b) Change in $\Omega_{\text{aragonite}}$ between 1991 and 2018 (2018 minus 1991). White lines represent the aragonite saturation horizon (ASH; $\Omega_{\text{aragonite}} = 1$) for 1991 (solid line) and 2018 (dashed line). White dots represent the sampling grid. Figure produced with Ocean Data View (Schlitzer, 2020).

Table 1

Layers and isopycnals delimiting them. The time-averaged pressure over the study period (Ref. Press., in dbar) is also given. ^a Potential density referenced to 0 dbar (σ_0), 1000 dbar (σ_1), and 2000 dbar (σ_2) for each basin. Values following the studies of Azetsu-Scott et al. (2003), Kieke et al. (2007), Pérez et al. (2008), and Yashayaev et al. (2008).

	Acronym	Name	Potential density (kg m^{-3}) ^a	Ref. Press. (dbar)
Irminger Basin	SPMW	Subpolar Mode Water	$\sigma_0 < 27.68$	259
	uLSW	upper Labrador Sea Water	$27.68 \leq \sigma_0 < 27.76$	792
			$27.76 \leq \sigma_0 < 27.81$	1440
	cLSW	classical Labrador Sea Water	$27.81 \leq \sigma_0 < 27.88$	2131
	ISOW	Iceland–Scotland Overflow Water	$27.88 \leq \sigma_0 < 27.88$	2766
$\sigma_0 \geq 27.88$				
Iceland Basin	SPMW	Subpolar Mode Water	$\sigma_0 < 27.68$	423
	uLSW	upper Labrador Sea Water	$\sigma_0 \geq 27.68$ and $\sigma_1 < 32.35$	999
			$\sigma_1 \geq 32.35$ and $\sigma_2 < 37$	1734
	cLSW	classical Labrador Sea Water	$\sigma_2 < 37$	2562
	ISOW	Iceland–Scotland Overflow Water	$\sigma_2 \geq 37$	

inverse of the standard error of the mean ($1/\sigma_x; \sigma_x = \sigma/\sqrt{N}$, where σ is the standard deviation of the samples within each layer and N is the number of samples within each layer) taking into account uncertainties in the input variables.

For further reference, the vertical sections of the mean in situ temperature, salinity, TA, DIC, C_{ant} , and C_{nat} during 1991–2018 are shown

in Fig. S1.

2.3. Projection of future changes in aragonite saturation states ($\Omega_{\text{aragonite}}$)

The response of ocean chemistry to increasing atmospheric mole fraction of CO_2 ($x\text{CO}_2$) is non-linear due to the decrease in the oceanic buffer capacity (Revelle factor; e.g., Sarmiento et al., 1995). Therefore, OA effects on the chemical environment can only be approximated as linear for small perturbations, i.e., short periods. To overcome this issue and to project OA effects on $\Omega_{\text{aragonite}}$ over long periods, the non-linear response of $\Omega_{\text{aragonite}}$ to the increase in atmospheric CO_2 can be approximated as linear by performing the study in terms of logarithms. Projecting future changes in ocean chemistry relative to atmospheric CO_2 rather than time has the advantage of being independent of the IPCC Shared Socioeconomic Pathways (SSP). The relationship between $\Omega_{\text{aragonite}}$ and atmospheric CO_2 also allows the computation of the pre-industrial $\Omega_{\text{aragonite}}$ (Table S4).

From our set of observations, we estimated future changes in $\Omega_{\text{aragonite}}$ through linear extrapolation of the observed relationship between $\ln(\Omega_{\text{aragonite}})$ versus $\ln(x\text{CO}_2)$, using mean annual atmospheric $x\text{CO}_2$ data from Mauna Loa, Hawaii (www.esrl.noaa.gov/gmd/ccgg/trends/). Our projections assume a thermodynamic equilibrium between $f\text{CO}_2$ in the atmosphere and seawater. As such, they should be taken as an upper bound of the expected changes, primarily because the CO_2 in the ocean lags that in the atmosphere (Orr et al., 2005). Our projections are based on linear extrapolation of the observed trends in $\Omega_{\text{aragonite}}$ during the 28 years from 1991 to 2018. These trends include variability imparted by inter-annual changes in remineralization rates, ventilation rates, and water mass circulation, which may not progress linearly.

3. Changes in $\Omega_{\text{aragonite}}$ and their potential drivers

Changes in $\Omega_{\text{aragonite}}$ are important for understanding how OA might impact marine ecosystems. During 1991–2018, upper-ocean and intermediate waters of the Irminger and Iceland Basins were supersaturated for aragonite ($\Omega_{\text{aragonite}} > 1$), while waters below 2500 m were undersaturated for aragonite ($\Omega_{\text{aragonite}} < 1$) (Fig. 2a). This vertical gradient of $\Omega_{\text{aragonite}}$ can be explained as a combination of the following processes: (a) the temperature and pressure dependence of K_{sp} ' (Mucci, 1983); (b) the changes in the TA / DIC ratio created by both biological activity (Carter et al., 2014) and the temperature-dependence of f_{CO_2} (Jiang et al., 2015); and (c) the temperature-dependence of the carbonic acid dissociation constants (Dickson and Millero, 1987). There were no appreciable differences in the $\Omega_{\text{aragonite}}$ fields of the Irminger and Iceland Basins despite observed differences in pH (García-Ibáñez et al., 2016). A layer with relatively low pH was observed at ~500 m depth in the Iceland Basin (García-Ibáñez et al., 2016, their Fig. 2c), a feature that is not present in the $\Omega_{\text{aragonite}}$ distribution due to the temperature-dependence of the chemical speciation of seawater CO_2 -carbonate chemistry species (e.g., Jiang et al., 2019, their Fig. S4). The speciation change combined with the change in K_{sp} ' with temperature and pressure (Mucci, 1983) buffers the observed change in pH in terms of $\Omega_{\text{aragonite}}$.

The study region is an area of low vertical $\Omega_{\text{aragonite}}$ gradient compared to the tropics and subtropics (e.g., Jiang et al., 2015). The $\Omega_{\text{aragonite}}$ values in the surface mixed layer ($\Omega_{\text{aragonite}} \approx 2$) are lower than those in subtropical and tropical areas ($\Omega_{\text{aragonite}} \approx 4$) (e.g., Jiang et al., 2015). The ISOW and DSOW layers are already undersaturated or close to undersaturation for aragonite, but they are supersaturated for calcite (another of the main CaCO_3 minerals formed by marine calcifying organisms; not shown), which is about 1.5 times less soluble than aragonite (Mucci, 1983).

Between 1991 and 2018, $\Omega_{\text{aragonite}}$ below 100 m depth decreased by a mean value of -0.11 ± 0.05 in both the Irminger and Iceland Basins (Fig. 2b). The upper SPMW layer and the recently ventilated uLSW layer of the Irminger Basin experienced the largest decrease in $\Omega_{\text{aragonite}}$,

which in general was higher than 0.15. The deep-water $\Omega_{\text{aragonite}}$ decreased by up to 0.1. The decrease in $\Omega_{\text{aragonite}}$ during 1991–2018 caused the ASH to shoal by an average of 400 m in the Irminger Basin and by 250 m in the Iceland Basin. The increase in $\Omega_{\text{aragonite}}$ observed in the upper 100 m is linked to the difference in surface temperature between 1991 and 2018 cruises, which took place in different seasons.

The $\Omega_{\text{aragonite}}$ shows significant decreasing trends in all the water-mass layers of both basins between 1991 and 2018 (Fig. 3; Table S2), mainly driven by changes in sDIC, generally led by the anthropogenic component (Fig. 4; Table S2), as was the case for the changes in pH (García-Ibáñez et al., 2016), as expected (Xue et al., 2020). Water-mass layers of both the Irminger and Iceland Basins gained DIC as atmospheric CO_2 increased, with convective processes providing an important pathway for transferring DIC to intermediate and deep layers (e.g., Pérez et al., 2008; Fröb et al., 2016). The main differences between the drivers for the changes in $\Omega_{\text{aragonite}}$ and pH are found in the influence of temperature and TA. García-Ibáñez et al. (2016) found that the main driver counteracting the pH decrease was TA. In this work the influence of TA as a counteracting factor of OA is lower due to a different separation of the physical and biogeochemical drivers performed in this work, highlighting that the contribution of TA to pH changes was mainly through changes in salinity. Temperature changes have opposite effects on $\Omega_{\text{aragonite}}$ and pH as a result of the temperature effect on the acid-base equilibrium of the CO_2 -carbonate system (Dickson and Millero, 1987), with increases in temperature causing a decrease in pH but an increase in $\Omega_{\text{aragonite}}$. Therefore, temperature increase dampens the decrease in $\Omega_{\text{aragonite}}$ caused by OA but reinforces the decrease in pH.

3.1. Changes in $\Omega_{\text{aragonite}}$ in mode waters (SPMW)

The upper layers, SPMWs, present the highest rate of $\Omega_{\text{aragonite}}$ decrease for 1991–2018 (Fig. 3; Table S2). Our rates of $\Omega_{\text{aragonite}}$ change in the SPMW layers of the Irminger ($-0.0052 \pm 0.0006 \text{ yr}^{-1}$) and Iceland ($-0.0049 \pm 0.0015 \text{ yr}^{-1}$) Basins are comparable with those in surface waters of the Irminger Sea time-series (Fig. 5a, green upward-

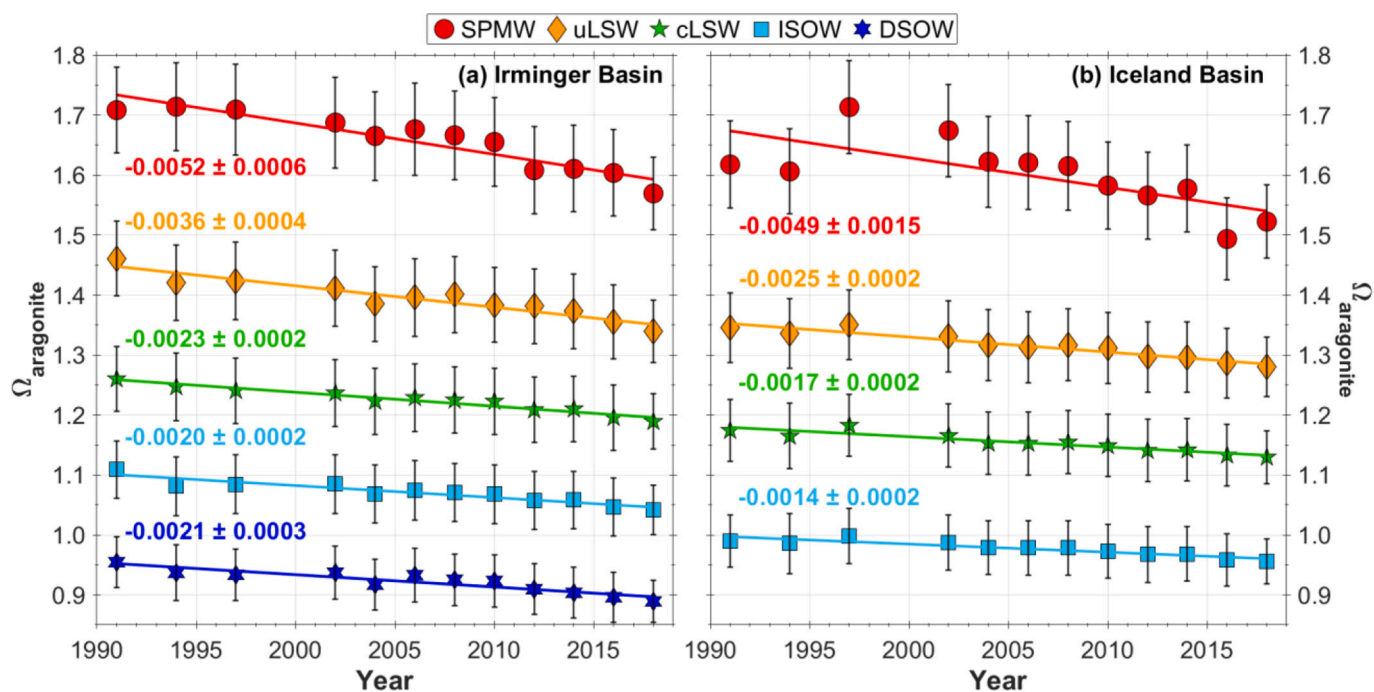


Fig. 3. Temporal evolution of the average aragonite saturation state ($\Omega_{\text{aragonite}}$) in the water-mass layers (Table 1) of the Irminger (a) and Iceland (b) Basins between 1991 and 2018. The error bars are the standard error of the mean ($\sigma_{\bar{x}} = \sigma/\sqrt{N}$, where σ is the standard deviation of the samples within each layer, and N is the number of samples within each layer), taking into account uncertainties in the input variables. Trends \pm standard error of the estimate (in yr^{-1}) are also given. All trends are statistically significant at the 99% level (p -value < 0.01).

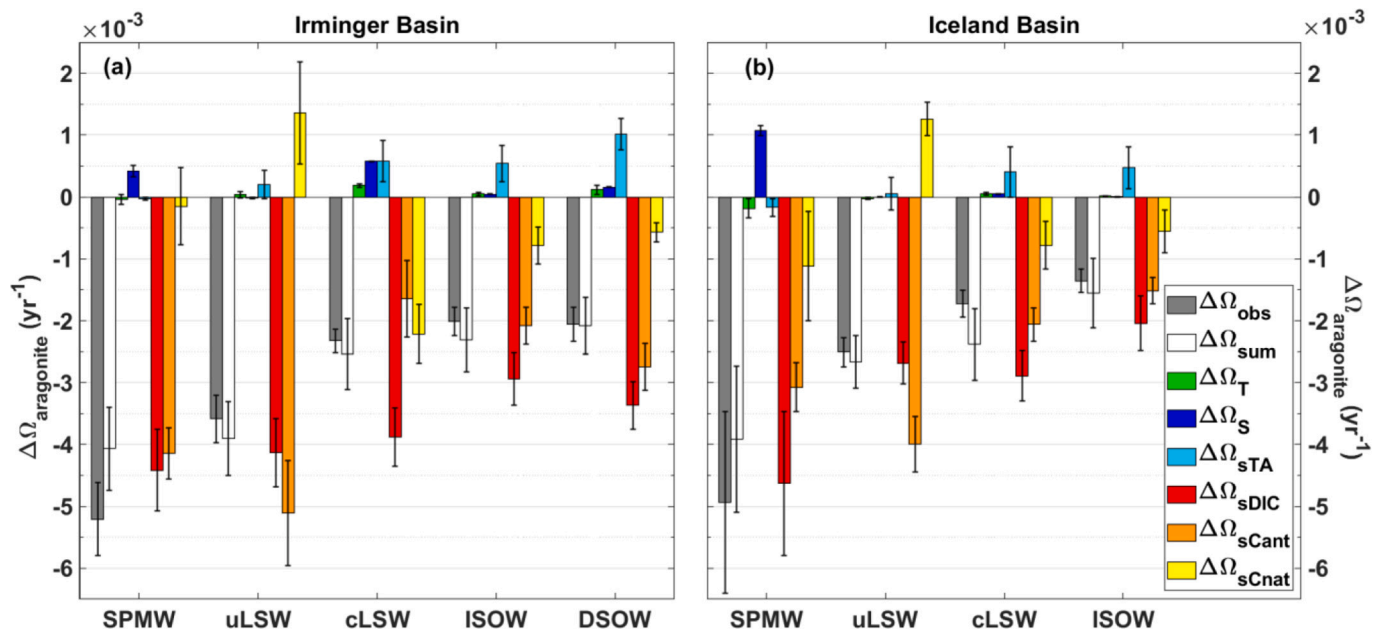


Fig. 4. Decomposition of the observed long-term trends (1991–2018) of the aragonite saturation state ($\Delta\Omega_{\text{obs}}$; grey bars) into the contributions of their main physical and chemical drivers in the water-mass layers (Table 1) of the Irminger (a) and Iceland (b) Basins: in situ temperature ($\Delta\Omega_T$; green bars), salinity ($\Delta\Omega_S$; navy bars), salinity-normalized total alkalinity ($\Delta\Omega_{\text{sTA}}$; light-blue bars), salinity-normalized total dissolved inorganic carbon ($\Delta\Omega_{\text{sDIC}}$; red bars), salinity-normalized anthropogenic CO_2 ($\Delta\Omega_{\text{sCant}}$; orange bars), and salinity-normalized natural DIC ($\Delta\Omega_{\text{sCnat}}$; yellow bars). Note that $\text{sDIC} = \text{sCant} + \text{sCnat}$ and, therefore, $\Delta\Omega_{\text{sDIC}} = \Delta\Omega_{\text{sCant}} + \Delta\Omega_{\text{sCnat}}$ (Section 2.2). The addition of the $\Omega_{\text{aragonite}}$ changes from each driver is also given ($\Delta\Omega_{\text{sum}}$; white bars). Trends are reported in ($\times 10^{-3}$) yr^{-1} , and the error bars represent the standard error of the estimate. (For interpretation of the references to colour in this figure legend, the reader is referred to the web version of this article.)

pointing triangle, IrS) and the Iceland Sea time-series (Fig. 5a, navy star), as well as at 200–500 m depth in the Iceland Sea and Norwegian Basin (Fig. 5a, white squares, IcS and NB, respectively), and in North Atlantic Central Waters of the North-East Atlantic Ocean (Fig. 5a, light-blue downward-pointing triangle, NACW). However, our rate of $\Omega_{\text{aragonite}}$ decrease of the SPMW layers is half those at 0–200 m depth in the Iceland Sea and Norwegian Basin (Fig. 5a, yellow squares). Note that the water masses in the Nordic Seas (Iceland Sea and Norwegian Basin) are not SPMW but Arctic Ocean waters (Olafsson et al., 2009), which have a higher rate of acidification (Fransner et al., 2020). Besides, the changes in $\Omega_{\text{aragonite}}$ for upper-ocean waters in the North Atlantic Subpolar Gyre region are subject to significant variability depending on the seasons and periods considered (Leseurre et al., 2020, their Fig. 4).

Comparing our results with those for time-series stations in the Atlantic Ocean outside our study region, our trends for mode waters are around half those reported for the surface layer at the Subtropical Atlantic time-series stations ESTOC (European Station for Time series in the Ocean at the Canary Islands; Fig. 5a, green upward-pointing triangle) and BATS (Bermuda Atlantic Time-series Study; Fig. 5a, pink left-pointing triangle), but comparable with those at CARIACO (Carbon Retention In A Colored Ocean; Fig. 5a, green upward-pointing triangle). Our $\Omega_{\text{aragonite}}$ rates of the SPMW layers are slightly lower than those found in surface waters of the Central North Pacific time-series station HOT (Hawaii Ocean Time-series) and of the subpolar South Pacific Munida Time-Series Transect (Fig. 5a, green upward-pointing triangles), but more than four times lower than in the upper 400 m of the subtropical South Pacific (Fig. 5a, black asterisk).

The differences in the rates of $\Omega_{\text{aragonite}}$ decrease in our study area and in the Nordic Seas (Iceland Sea time-series) and subtropical and tropical regions are expected due to the temperature-dependence of $\Omega_{\text{aragonite}}$ (e.g., Carter et al., 2014; Takahashi et al., 2014, their Fig. 17; Jiang et al., 2015). The temperature-dependence of $\Omega_{\text{aragonite}}$ originates from the temperature-dependence of K_{sp}' (Mucci, 1983) and the temperature-dependence of $[\text{CO}_3^{2-}]$, which results from the temperature-dependence of both the carbonic acid dissociation

constants (Dickson and Millero, 1987) and $f\text{CO}_2$ that influences the TA / DIC ratio (Jiang et al., 2015).

The rates of $\Omega_{\text{aragonite}}$ decrease in the SPMW layers are mainly driven by changes in sDIC (Fig. 4; Table S2). $\Delta\Omega_{\text{sDIC}}$ values are largely caused by C_{ant} uptake (solubility pump). The increase in salinity partly counteracts the effect of the sDIC, reducing the $\Omega_{\text{aragonite}}$ decrease by up to 22%. The salinization of SPMW (Yashayaev and Dickson, 2008) likely results from the transport of a higher proportion of saline subtropical waters into the North Atlantic Subpolar Gyre since the mid-1990s (e.g., Flatau et al., 2003; Häkkinen and Rhines, 2004; Böning et al., 2006; Thierry et al., 2008). The impacts of temperature and sTA on the $\Omega_{\text{aragonite}}$ decrease of the SPMW layers are negligible. The addition of the $\Omega_{\text{aragonite}}$ changes due to each driver ($\Delta\Omega_{\text{sum}}$) reproduces $\sim 80\%$ of the observed $\Omega_{\text{aragonite}}$ trends ($\Delta\Omega_{\text{obs}}$) in the SPMW layers, with no significant difference between $\Delta\Omega_{\text{sum}}$ and $\Delta\Omega_{\text{obs}}$. The $\Delta\Omega_{\text{sum}}$ does not fully reproduce $\Delta\Omega_{\text{obs}}$ because of temporal variability in $\Omega_{\text{aragonite}}$ (Fig. 3) as well as in the drivers of $\Delta\Omega_{\text{aragonite}}$ (Fig. S2), and because of the simplification of the first-order Taylor expansion.

3.2. Changes in $\Omega_{\text{aragonite}}$ in intermediate waters (uLSW and cLSW)

During 1991–2018 the $\Omega_{\text{aragonite}}$ of uLSW decreased by $-0.0036 \pm 0.0004 \text{ yr}^{-1}$ in the Irminger Basin and by $-0.0025 \pm 0.0002 \text{ yr}^{-1}$ in the Iceland Basin (Fig. 3; Table S2). Our estimates of $\Delta\Omega_{\text{aragonite}}$ for the uLSW layers are twice those reported for water at 1000 m depth for the entire North Atlantic Ocean (Fig. 5b, orange right-pointing triangle). However, the rate of the $\Omega_{\text{aragonite}}$ decrease of uLSW is lower than that of Arctic Intermediate Waters (500–1000 m depth) in the Iceland Sea and Norwegian Basin (Fig. 5b, yellow squares, IcS and NB, respectively). The rate of the $\Omega_{\text{aragonite}}$ decrease of uLSW is also lower than that of Mediterranean Water in the North-East Atlantic Ocean (Fig. 5b, light-blue downward-pointing triangle, MW).

The $\Omega_{\text{aragonite}}$ decrease of the uLSW layers is mainly driven by C_{ant} uptake (Fig. 4; Table S2), with changes in C_{nat} significantly counteracting the decrease in $\Omega_{\text{aragonite}}$ in the Iceland Basin. The increase in

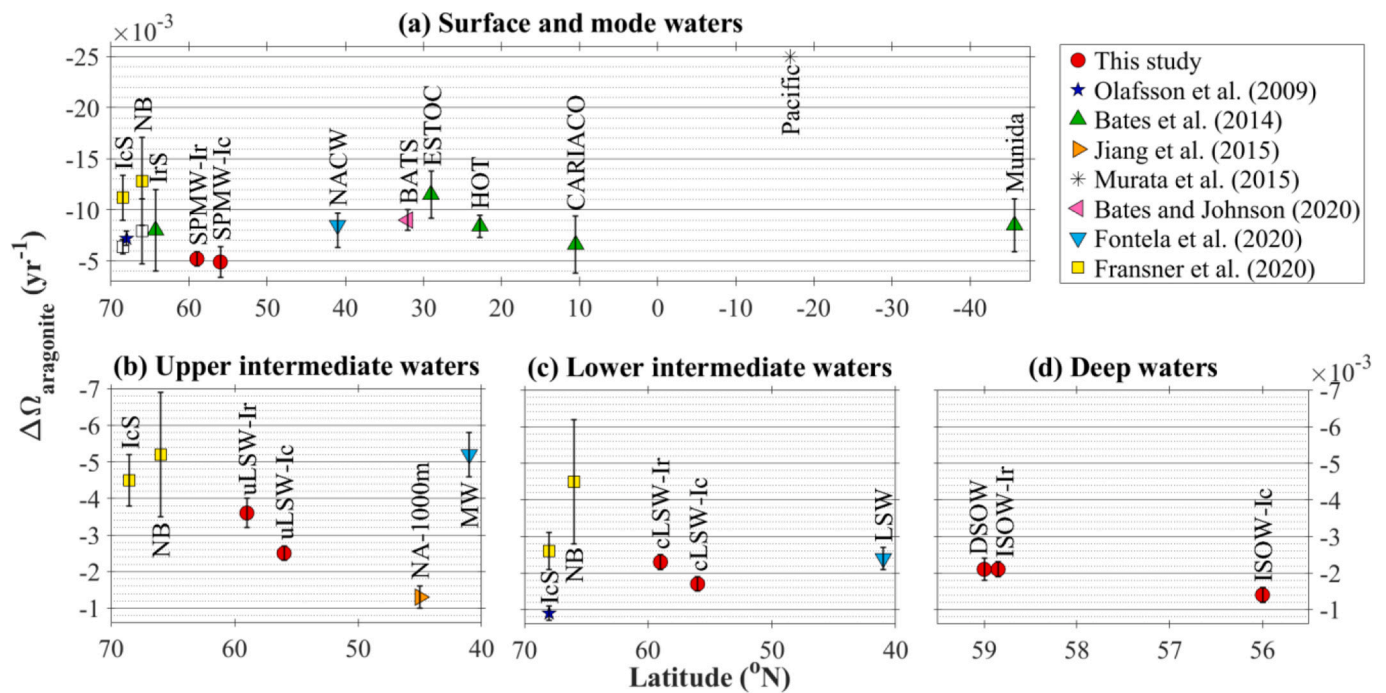


Fig. 5. Rates of change in aragonite saturation state ($\Delta\Omega_{\text{aragonite}}$; in yr^{-1}) versus latitude ($^{\circ}\text{N}$) for (a) surface and mode waters, (b) upper intermediate waters, (c) lower intermediate waters, and (d) deep waters in our study and those reported by previous studies (Table S3). Red dots represent $\Delta\Omega_{\text{aragonite}}$ for 1991–2018 in the water-mass layers (Table 1) of the Irminger (-Ir) and Iceland (-Ic) Basins from this study. Green upward-pointing triangles (Bates et al., 2014) represent $\Delta\Omega_{\text{aragonite}}$ in surface waters of (a) the Irminger Sea time-series (IrS; 64.3°N 28°W) for 1983–2014, ESTOC (29.04°N 15.50°W) for 1995–2014, HOT (22.45°N 158°W) for 1988–2014, CARIACO (10.5°N 64.67°W) for 1995–2014, and Munida Time-Series Transect (45.7°S 171.5°E) for 1998–2014. Navy stars (Olafsson et al., 2009) represent $\Delta\Omega_{\text{aragonite}}$ for 1985–2008 in (a) surface waters and (c) waters deeper than 1500 m of the Iceland Sea time-series (IcS; 68°N 12.66°W). Squares (Fransner et al., 2020) represent $\Delta\Omega_{\text{aragonite}}$ for 1981–2019 in the Iceland Sea (IcS; $\sim 67\text{--}70^{\circ}\text{N}$ $\sim 10\text{--}15^{\circ}\text{W}$) and the Norwegian Basin (NB; $\sim 64\text{--}67^{\circ}\text{N}$ $\sim 5^{\circ}\text{W}\text{--}2^{\circ}\text{E}$) at (a) 0–200 m depth (yellow squares), 200–500 m depth (white squares), (b) 500–1000 m depth (yellow squares), and (c) 1000–2000 m depth (yellow squares). Light-blue downward-pointing triangles (Fontela et al., 2020) represent $\Delta\Omega_{\text{aragonite}}$ for 1997–2018 in the North-East Atlantic Ocean ($40\text{--}45^{\circ}\text{N}$ $9\text{--}36^{\circ}\text{W}$) for (a) North Atlantic Central Water (NACW), (b) Mediterranean Water (MW), and (c) Labrador Sea Water (LSW). The pink left-pointing triangle (Bates and Johnson, 2020) represents $\Delta\Omega_{\text{aragonite}}$ for 1983–2020 in (a) surface waters at BATS (32°N 64°W). The black asterisk (Murata et al., 2015) represents $\Delta\Omega_{\text{aragonite}}$ for 1994–2009 in (a) the upper 400 m of the subtropical South Pacific (Pacific; $\sim 17\text{--}25^{\circ}\text{S}$ $\sim 80\text{--}168^{\circ}\text{W}$). The orange right-pointing triangle (Jiang et al., 2015) represents $\Delta\Omega_{\text{aragonite}}$ for 1989–2010 for (c) water at 1000 m depth in the entire North Atlantic Ocean (NA-1000 m). Trends are reported in $(\times 10^{-3}) \text{yr}^{-1}$, and the error bars represent the standard error of the estimate. Note the different scales of the subplots and the reverse y-scale. (For interpretation of the references to colour in this figure legend, the reader is referred to the web version of this article.)

$\Omega_{\text{aragonite}}$ of uLSW due to C_{nat} indicates that the uLSW layer was occasionally ventilated (e.g., Våge et al., 2009; Yashayaev and Loder, 2009, 2016; Kieke and Yashayaev, 2015; Fröb et al., 2016). The impacts of temperature, salinity, and sTA on $\Omega_{\text{aragonite}}$ trends of uLSW are small-to-negligible (with the counteracting effect of sTA on $\Delta\Omega_{\text{aragonite}}$ of uLSW as small as 2–6%).

For the cLSW layers, the $\Omega_{\text{aragonite}}$ decreased by $-0.0017 \pm 0.0002 \text{ yr}^{-1}$ in the Iceland Basin and by $-0.0023 \pm 0.0002 \text{ yr}^{-1}$ in the Irminger Basin for 1991–2018 (Fig. 3; Table S2). Our estimates of $\Delta\Omega_{\text{aragonite}}$ in the cLSW layers are comparable with those in the LSW of the North-East Atlantic Ocean (Fig. 5c, light-blue downward-pointing triangle, LSW). The rates of decrease in $\Omega_{\text{aragonite}}$ of the cLSW layers are double the rate reported for waters deeper than 1500 m at the Iceland Sea time-series station (Fig. 5c, navy star), but similar to those at 1000–2000 m depth in the Iceland Sea (Fig. 5c, yellow square, IcS). However, the rate of decrease in $\Omega_{\text{aragonite}}$ of cLSW is half that of the Arctic Deep Waters (1000–2000 m depth) of the Norwegian Basin (Fig. 5c, yellow square, NB).

The DIC changes of the cLSW layers are the main contributors to the observed $\Omega_{\text{aragonite}}$ decrease (Fig. 4; Table S2), with changes in C_{nat} reinforcing the decrease in $\Omega_{\text{aragonite}}$ caused by C_{ant} uptake in the Irminger Basin. The higher influence of C_{nat} in the $\Omega_{\text{aragonite}}$ decline of the cLSW layers compared to other layers is likely the result of the aging of this water mass (accumulation of DIC from remineralized organic matter) after its last strong formation event in the mid-1990s (e.g.,

Lazier et al., 2002; Azetsu-Scott et al., 2003; Kieke et al., 2007; Yashayaev, 2007). The formation history of cLSW can also explain the attenuation in the $\Omega_{\text{aragonite}}$ decrease through changes in temperature and salinity. Enhanced ventilation towards the mid-to-late 1980s fostered the rapid formation of a large volume of cLSW in the Labrador Sea and transported cold waters from the surface into intermediate waters. The shutdown of the cLSW production in the mid-1990s (Lazier et al., 2002; Kieke et al., 2006; Rhein et al., 2007; Yashayaev et al., 2008) caused the warming and salinization of this layer due to lateral mixing with surrounding waters, such as SPMWs, which have experienced an increase in salinity (Yashayaev and Dickson, 2008). These effects were more remarkable for the cLSW layer in the Irminger Basin than in the Iceland Basin due to the proximity of the former to the Labrador Sea. Therefore, the OA signal of the cLSW layers is reinforced by a reduction in ventilation (Chen et al., 2017).

Since CWCs mainly inhabit the LSW layers, we estimated the upward migration of the $\Omega_{\text{aragonite}}$ isolines that may ultimately affect the metabolic status of aragonitic CWCs (e.g., Thresher et al., 2011; Hennige et al., 2014). The decrease in $\Omega_{\text{aragonite}}$ of the uLSW layers led to a shoaling of the $\Omega_{\text{aragonite}}$ isolines at a rate of 34 m yr^{-1} in the Irminger Basin and 23 m yr^{-1} in the Iceland Basin. For the cLSW layers, the $\Omega_{\text{aragonite}}$ isolines shoaled at a rate of 10 m yr^{-1} in the Irminger Basin and 6 m yr^{-1} in the Iceland Basin. The $10\text{--}15 \text{ m yr}^{-1}$ shoaling rate of the ASH estimated for the center of the Irminger Sea for 1991–2016 by Pérez et al. (2018) are in agreement with ours for the cLSW in the Irminger and

Iceland Basins. In comparison, the 6 m yr^{-1} shoaling of the $\Omega_{\text{aragonite}}$ isolines of the cLSW layer of the Iceland Basin is slightly higher than the 4 m yr^{-1} shoaling trend reported for the Iceland Sea for 1985–2008 (Olafsson et al., 2009), and the 5.2 m yr^{-1} shoaling trend for the subtropical South Pacific Ocean for 1994–2009 at 400 m depth (Murata et al., 2015). The shoaling of the $\Omega_{\text{aragonite}}$ isolines of the uLSW layers is 12–17 times higher than the $2.0 \pm 0.7 \text{ m yr}^{-1}$ estimated for the $\Omega_{\text{aragonite}}$ isoline of 1.3 (contour within the uLSW; Fig. 2) in the high latitudes of the Southern Hemisphere for 1992–2011 (Williams et al., 2015). The cause of the higher shoaling rates of $\Omega_{\text{aragonite}}$ in our analysis compared to those reported by Williams et al. (2015) is three-fold. First, Williams et al. (2015) evaluated the changes in $\Omega_{\text{aragonite}}$ between only two years (1992 versus 2011 or 2005 versus 2011), being, therefore, more sensitive to inter-annual variability than our trend analysis. Second, Williams et al. (2015) only observed an anthropogenic signal in the upper 100 m, while the changes in $\Omega_{\text{aragonite}}$ in the waters below the mixed layer result from either a slowdown in circulation or decreased ventilation. Therefore, the Pacific sector of the Southern Ocean was less affected by the anthropogenic signal than our study region, the Subpolar North Atlantic, causing the shoaling rates in the Pacific sector of the Southern Ocean to be significantly smaller than those in the Subpolar North Atlantic. Finally, when comparing shoaling rates of $\Omega_{\text{aragonite}}$ one should note that they are a function of both the OA rates and the vertical gradient in the $\Omega_{\text{aragonite}}$; therefore, similar OA signals could generate different shoaling rates depending on the $\Omega_{\text{aragonite}}$ gradient.

3.3. Changes in $\Omega_{\text{aragonite}}$ in deep waters (ISOW and DSOW)

This study provides the first published trends of $\Omega_{\text{aragonite}}$ in the deep waters of the Irminger and Iceland Basins. During 1991–2018, $\Omega_{\text{aragonite}}$ decreased by $-0.0014 \pm 0.0002 \text{ yr}^{-1}$ in the ISOW layer in the Iceland

Basin, and by $-0.0020 \pm 0.0002 \text{ yr}^{-1}$ and $-0.0021 \pm 0.0003 \text{ yr}^{-1}$ in the ISOW and DSOW layers of the Irminger Basin, respectively (Fig. 3; Table S2). The entrainment of intermediate waters into the overflow layers (van Aken, 2000; Dickson et al., 2002; Sarafanov et al., 2010) is likely to transfer the OA signal from intermediate to deep waters, hence, making the $\Omega_{\text{aragonite}}$ trends of the ISOW and DSOW layers similar to those of the cLSW layers (Fig. 5c,d). The entrainment of intermediate waters into the overflow waters may explain why we observe a statistically significant rate of $\Omega_{\text{aragonite}}$ decrease in the deep waters of the Irminger and Iceland Basins while no significant rate of $\Omega_{\text{aragonite}}$ decrease was found in the deep waters of the Norwegian Basin (Fransner et al., 2020).

Changes in DIC and TA constitute the primary drivers of the temporal evolution of $\Omega_{\text{aragonite}}$ in the deep waters (Fig. 4; Table S2), with changes in sTA significantly offsetting the reduction in $\Omega_{\text{aragonite}}$ caused by the increase in sDIC for the Irminger Basin. Changes in temperature and salinity in the overflow waters did not significantly affect $\Delta\Omega_{\text{aragonite}}$. The substantial influence of C_{ant} on the $\Omega_{\text{aragonite}}$ decrease in the overflow layers (DSOW and ISOW) stands out, with significant parallel pH decreases in these water-mass layers (García-Ibáñez et al., 2016). The $\Omega_{\text{aragonite}}$ decrease due to C_{nat} for ISOW and DSOW could derive from the increase in TA from excess carbonate mineral dissolution and/or from the mixing with cLSW and relatively old North Atlantic Deep Water, with high DIC accumulation from organic matter remineralization (Fig. S1e). The increase in sTA in the overflow waters, counteracting the decrease in $\Omega_{\text{aragonite}}$, may have been transmitted from SPMW and LSW through entrainment (Yashayaev and Dickson, 2008; Sarafanov et al., 2010; Hansen et al., 2016).

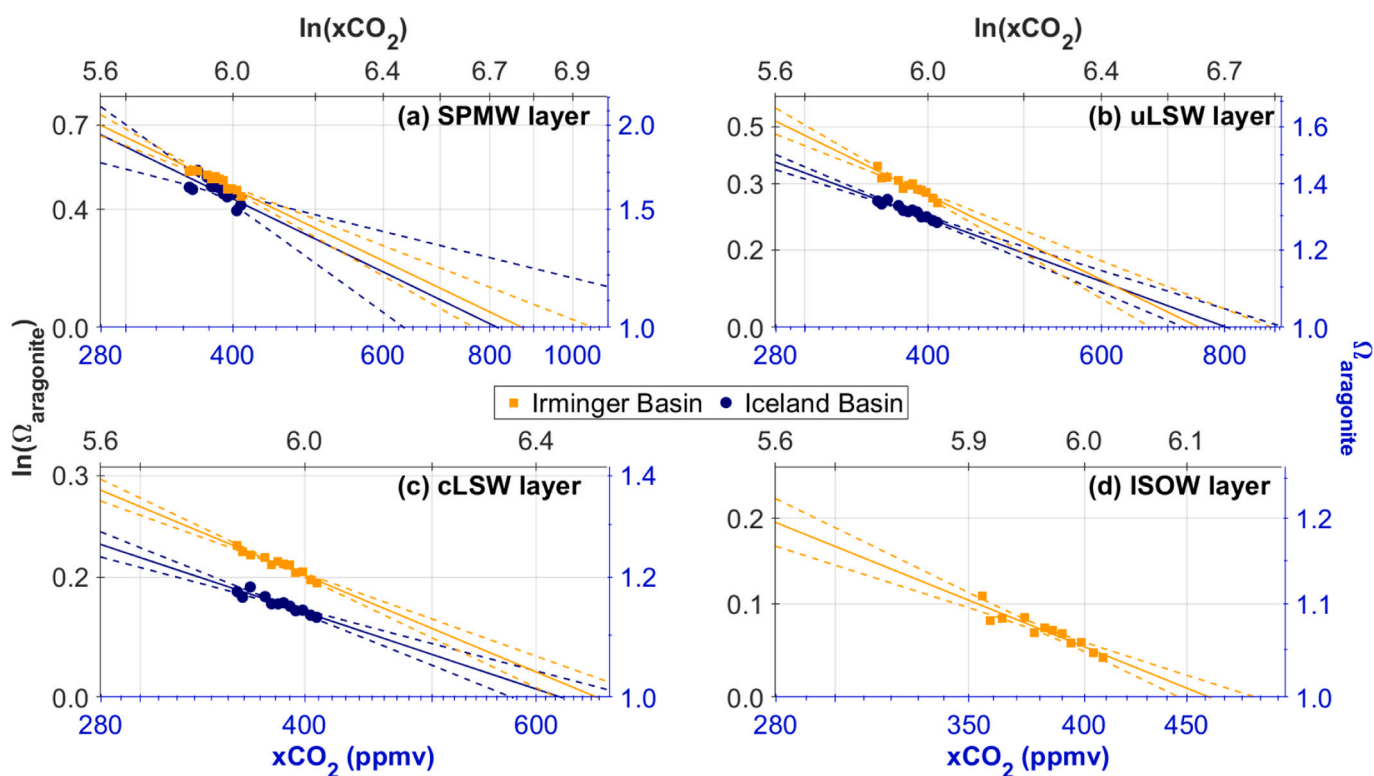


Fig. 6. Projections of the observed long-term trends (1991–2018) of the natural logarithm of aragonite saturation state ($\ln(\Omega_{\text{aragonite}})$) versus the natural logarithm of the atmospheric mole fraction of CO_2 at the year of the cruise ($\ln(x\text{CO}_2)$) per water-mass layer (Table 1) in the Irminger (orange squares) and Iceland (navy dots) Basins. Solid lines represent the weighted linear trend of $\ln(\Omega_{\text{aragonite}})$ versus $\ln(x\text{CO}_2)$, and dashed lines represent the error of the estimate. Right y-axes represent the $\Omega_{\text{aragonite}}$ values corresponding to the $\ln(\Omega_{\text{aragonite}})$ values on the left y-axes. Lower x-axes represent the $x\text{CO}_2$ values (in ppmv) corresponding to the $\ln(x\text{CO}_2)$ on the upper x-axes of the subplots. (For interpretation of the references to colour in this figure legend, the reader is referred to the web version of this article.)

4. Projected future changes in $\Omega_{\text{aragonite}}$

Our projections of future $\Omega_{\text{aragonite}}$ relative to atmospheric $x\text{CO}_2$ indicate that the entire water column of the Irminger and Iceland Basins will likely be undersaturated for aragonite by the time $x\text{CO}_2$ reaches 876 ± 83 ppmv (approximately twice the present atmospheric $x\text{CO}_2$; Fig. 6; Table S4). Atmospheric $x\text{CO}_2$ will likely reach 876 ppmv before the end of the century according to SSP5 (Riahi et al., 2017), which is the SSP with the highest emissions (the only SSP that results in a radiative forcing pathway close to the highest Representative Concentration Pathway RCP8.5; Kriegler et al., 2017) and the one we have followed most closely (e.g., Sanford et al., 2014). Numerical models based on RCP8.5 also project aragonite undersaturation in the North Atlantic north of 50°N by 2100 (Feely et al., 2009; Matear and Lenton, 2014). The intermediate waters of the Irminger and Iceland Basins will become undersaturated for aragonite much sooner. The uLSW layers will likely become undersaturated for aragonite when in equilibrium with atmospheric $x\text{CO}_2$ of 757–808 ppmv (Fig. 6b; Table S4). The cLSW layers will be close to undersaturation for aragonite when in equilibrium with an atmospheric $x\text{CO}_2$ of 558 ppmv (an $x\text{CO}_2$ level corresponding to 2°C global warming for the SSP5 Baseline Marker; Riahi et al., 2017), reaching aragonite undersaturation when atmospheric $x\text{CO}_2$ reaches 628–669 ppmv (Fig. 6c; Table S4). The ISOW layer of the Irminger Basin will be undersaturated for aragonite when in equilibrium with an atmospheric $x\text{CO}_2$ of 463 ppmv (Fig. 6d; Table S4), 52 ppmv above the current atmospheric $x\text{CO}_2$ level.

Aragonite undersaturation of the cLSW and ISOW layers will create a chemically unfavorable state for CWCs that inhabit these depths (Fig. 1; e.g., Maier et al., 2009; Ragazzola et al., 2012). Physiological acclimation to OA (higher levels of CO_2) was observed in *Lophelia pertusa* during long-term incubations (e.g., Form and Riebesell, 2012; Hennige et al., 2015). But the exposed bases of the reefs become more susceptible to bio-erosion and mechanical damage when exposed to higher levels of CO_2 , with a corresponding reduction in the structural integrity of the reef (e.g., Hennige et al., 2015) that could ultimately cause reef collapse. Therefore, the potential increase in the dissolution of the dead bases of the reefs could lead to a net loss of CWC reefs, rather than the reduction in calcification rates of the live coral (Hennige et al., 2015). The systemic weakening and ultimate loss of the foundation framework from OA would prevent future reef and mound growth and lead to an ecosystem-scale habitat loss for existing CWC reefs (Hennige et al., 2020).

5. Summary

The gradual reduction over time of $\Omega_{\text{aragonite}}$ in the Subpolar North Atlantic Ocean was assessed from observations in the Irminger and Iceland Basins spanning the last three decades (1991–2018). Upper-ocean and intermediate waters of the Iceland and Irminger Basins were supersaturated for the aragonite form of CaCO_3 , while waters below 2500 m depth were undersaturated. The entire water column of both basins showed statistically significant decreasing $\Omega_{\text{aragonite}}$ trends, with the greatest decrease in upper-ocean waters. The $\Omega_{\text{aragonite}}$ decrease in intermediate waters, which 44% of the CWC reefs of the study region inhabit, has caused the $\Omega_{\text{aragonite}}$ isolines to shoal at a rate of $6\text{--}34\text{ m yr}^{-1}$ in the Irminger and Iceland Basins. We attribute the $\Omega_{\text{aragonite}}$ changes mainly to the oceanic C_{ant} uptake, reinforced in the cLSW layers by increases in net remineralization as ventilation rates decreased and mean water age increased. The increase in salinity (and thus in $[\text{Ca}^{2+}]$) in the SPMW layers reduced the $\Omega_{\text{aragonite}}$ decrease resulting from the increase in DIC. For the uLSW layers, its recent ventilation counteracted the decrease in $\Omega_{\text{aragonite}}$ from C_{ant} uptake. For cLSW and deep waters, the $\Omega_{\text{aragonite}}$ decreases caused by increases in DIC were offset by increases in TA. Taking advantage of the observed $\Omega_{\text{aragonite}}$ change for 1991–2018, we inferred its future change for increases in atmospheric CO_2 . Our projections suggest that the entire water column of both basins would be undersaturated for aragonite when in equilibrium with an atmospheric

$x\text{CO}_2$ of ~ 880 ppmv (which will be reached by the end of the century according to the SSP5 climate scenario), which is in agreement with projections from numerical models. However, intermediate layers between 1000 and 2000 m depth would reach aragonite undersaturation more rapidly, when in equilibrium with an atmospheric $x\text{CO}_2$ exceeding ~ 630 ppmv, an $x\text{CO}_2$ level slightly above that corresponding to 2°C global warming. The future aragonite undersaturation of the intermediate layers is likely to affect the distribution, calcification rates, and structural stability of the CWC reefs, important hotspots of biodiversity in the North Atlantic Ocean.

Author contributions

MIGI wrote the manuscript and prepared the figures. MIGI, MF, and AV contributed to the acquisition of data. MIGI, NRB, DCEB, MF, and AV discussed the results and reviewed the manuscript and supporting information.

Data availability statement

Data supporting the conclusions of this article are available through the authors and GLODAPv2.2020 (Olsen et al., 2020).

Declaration of Competing Interest

The authors declare no competing financial interest.

Acknowledgements

We are grateful to the captains, crew, and researchers who contributed to the acquisition and processing of hydrographic and ocean carbon data. The research leading to these results was supported through the EU FP7 project CARBOCHANGE “Changes in carbon uptake and emissions by oceans in a changing climate”, which received funding from the European Commission’s Seventh Framework Programme under grant agreement No 264879. For this work, M.I. García-Ibáñez and A. Velo were supported by the BOCATS2 Project (PID2019-104279GB-C21) co-funded by the Spanish Government and the Fondo Europeo de Desarrollo Regional (FEDER). M.I. Garcia-Ibanez was also supported by the UK’s Natural Environment Research Council CUSTARD grant [NE/P021263/1], part of the RoSES programme. N.R. Bates was funded by National Science Foundation award (OCE-1258622). M. Fontela was funded by Portuguese national funds from the FCT–Foundation for Science and Technology through project UID/Multi/04326/2019 and CEECINST/00114/2018. This project has also received funding from the European Union’s Horizon 2020 research and innovation programme under grant agreement No 820989 (project COMFORT, Our common future ocean in the Earth system – Quantifying coupled cycles of carbon, oxygen, and nutrients for determining and achieving safe operating spaces with respect to tipping points). The work reflects only the author’s/authors’ view; the European Commission and their executive agency are not responsible for any use that may be made of the information the work contains. We thank Fiz F. Pérez for his constructive and useful discussion that greatly helped to improve the paper. We thank the two anonymous reviewers whose insightful comments and suggestions helped improve and clarify this manuscript.

Appendix A. Supplementary data

Supplementary data to this article can be found online at <https://doi.org/10.1016/j.gloplacha.2021.103480>.

References

- Álvarez, M., Ríos, A.F., Pérez, F.F., Bryden, H.L., Rosón, G., 2003. Transports and budgets of total inorganic carbon in the subpolar and temperate North Atlantic. *Glob. Biogeochem. Cycles* 17, 1002. <https://doi.org/10.1029/2002GB001881>.
- Andersson, A.J., Mackenzie, F.T., Gattuso, J.-P., 2011. Effects of ocean acidification on benthic processes, organisms, and ecosystems. In: Gattuso, J.-P., Hansson, L. (Eds.), *Ocean Acidification*. Oxford University Press, New York, pp. 122–153.
- Archer, D., Eby, M., Brovkin, V., Ridgwell, A., Cao, L., Mikolajewicz, U., Caldeira, K., Matsumoto, K., Munhoven, G., Montenegro, A., Tokos, K., . Atmospheric lifetime of fossil fuel carbon dioxide. *Annu. Rev. Earth Planet. Sci.* 37, 117–134. <https://doi.org/10.1146/annurev.earth.031208.100206>.
- Azetsu-Scott, K., Jones, E.P., Yashayaev, I., Gershay, R.M., 2003. Time series study of CFC concentrations in the Labrador Sea during deep and shallow convection regimes (1991–2000). *J. Geophys. Res.* 108, 3354. <https://doi.org/10.1029/2002JC001317>.
- Bates, N.R., Johnson, R.J., 2020. Acceleration of ocean warming, salinification, deoxygenation and acidification in the surface subtropical North Atlantic Ocean. *Commun. Earth Environ.* 1, 33. <https://doi.org/10.1038/s43247-020-00030-5>.
- Bates, N., Astor, Y., Church, M., Currie, K., Dore, J., González-Dávila, M., Lorenzoni, L., Müller-Karger, F., Olafsson, J., Santana-Casiano, M., 2014. A time-series view of changing ocean chemistry due to ocean uptake of anthropogenic CO₂ and ocean acidification. *Oceanography* 27, 126–141. <https://doi.org/10.5670/oceanog.2014.16>.
- Böning, C.W., Scheinert, M., Dengg, J., Biastoch, A., Funk, A., 2006. Decadal variability of subpolar gyre transport and its reverberation in the North Atlantic overturning. *Geophys. Res. Lett.* 33, L21S01. <https://doi.org/10.1029/2006GL026906>.
- Carter, B.R., Toggweiler, J.R., Key, R.M., Sarmiento, J.L., 2014. Processes determining the marine alkalinity and calcium carbonate saturation state distributions. *Biogeosciences* 11, 1–14. <https://doi.org/10.5194/bg-11-7349-2014>.
- Chen, C.-T.A., Lui, H.-K., Hsieh, C.-H., Yanagi, T., Kosugi, N., Ishii, M., Gong, G.-C., 2017. Deep oceans may acidify faster than anticipated due to global warming. *Nat. Clim. Chang.* 7, 890–894. <https://doi.org/10.1038/s41558-017-0003-y>.
- Daniault, N., Mercier, H., Lherminier, P., Sarafanov, A., Falina, A., Zunino, P., Pérez, F.F., Ríos, A.F., Ferron, B., Huck, T., Thierry, V., Gladyshev, S., 2016. The northern North Atlantic Ocean mean circulation in the early 21st century. *Prog. Oceanogr.* 146, 142–158. <https://doi.org/10.1016/j.poccean.2016.06.007>.
- DeVries, T., 2014. The oceanic anthropogenic CO₂ sink: storage, air-sea fluxes, and transports over the industrial era. *Glob. Biogeochem. Cycles* 28, 631–647. <https://doi.org/10.1002/2013GB004739>.
- Dickson, A.G., 1990. Standard potential of the reaction: AgCl(s) + 12H₂(g) = Ag(s) + HCl(aq), and the standard acidity constant of the ion HSO₄⁻ in synthetic sea water from 273.15 to 318.15 K. *J. Chem. Thermodyn.* 22, 113–127. [https://doi.org/10.1016/0021-9614\(90\)90074-z](https://doi.org/10.1016/0021-9614(90)90074-z).
- Dickson, A., Millero, F., 1987. A comparison of the equilibrium constants for the dissociation of carbonic acid in seawater media. *Deep-Sea Res.* 34, 1733–1743. [https://doi.org/10.1016/0198-0149\(87\)90021-5](https://doi.org/10.1016/0198-0149(87)90021-5).
- Dickson, A.G., Sabine, C.L., Christian, J.R. (Eds.), 2007. *Guide to best practices for ocean CO₂ measurements*. *PICES Special Publication* 3 (191 pp).
- Dickson, B., Yashayaev, I., Meincke, J., Turrell, B., Dye, S., Holfort, J., 2002. Rapid freshening of the deep North Atlantic Ocean over the past four decades. *Nature* 416, 832–837. <https://doi.org/10.1038/416832a>.
- Doney, S.C., Busch, D.S., Cooley, S.R., Kroeker, K.J., 2020. The impacts of ocean acidification on marine ecosystems and reliant human communities. *Annu. Rev. Environ. Resour.* 45, 83–112. <https://doi.org/10.1146/annurev-environ-012320-083019>.
- Fajar, N.M., Guallart, E.F., Steinfeldt, R., Ríos, A.F., Pelegrí, J.L., Pelejero, C., Calvo, E., Pérez, F.F., 2015. Anthropogenic CO₂ changes in the Equatorial Atlantic Ocean. *Prog. Oceanogr.* 134, 256–270. <https://doi.org/10.1016/j.poccean.2015.02.004>.
- Feely, R.A., Sabine, C.L., Lee, K., Berelson, W., Kleypas, J., Fabry, V.J., Millero, F.J., 2004. Impact of anthropogenic CO₂ on the CaCO₃ system in the oceans. *Science* 305, 362–366. <https://doi.org/10.1126/science.1097329>.
- Feely, R.A., Doney, S.C., Cooley, S.R., 2009. Ocean acidification: present and future changes in a high-CO₂ world. *Oceanography* 22, 36–47. <https://doi.org/10.5670/oceanog.2009.95>.
- Flatau, M.K., Talley, L., Niiler, P.P., 2003. The North Atlantic Oscillation, surface current velocities, and SST changes in the subpolar North Atlantic. *J. Clim.* 16, 2355–2369. <https://doi.org/10.1175/2787.1>.
- Fontela, M., Pérez, F., Carracedo, L., Padín, X., Velo, A., García-Ibañez, M., Lherminier, P., 2020. The Northeast Atlantic is running out of excess carbonate in the horizon of cold-water coral communities. *Sci. Rep.* 10, 14714. <https://doi.org/10.1038/s41598-020-71793-2>.
- Form, A.U., Riebesell, U., 2012. Acclimation to ocean acidification during long-term CO₂ exposure in the cold-water coral *Lophelia pertusa*. *Glob. Chang. Biol.* 18, 843–853. <https://doi.org/10.1111/j.1365-2486.2011.02583.x>.
- Franser, F., Fröb, F., Tjiputra, J., Chierici, M., Fransson, A., Jeansson, E., Johannessen, T., Jones, E., Lauvset, S.K., Ólafsdóttir, S.R., Omar, A., Skjelvan, I., Olsen, A., 2020. Nordic seas acidification. *Biogeosci. Discuss.* <https://doi.org/10.5194/bg-2020-339> in review.
- Freiwald, A., Rogers, A., Hall-Spencer, J., Guinotte, J.M., Davies, A.J., Yesson, C., Martin, C.S., Weatherdon, L.V., 2017. Global distribution of cold-water corals (version 5.0). In: Fifth update to the dataset in Freiwald et al. (2004) by UNEP-WCMC, in collaboration with Andre Freiwald and John Guinotte. UN Environment World Conservation Monitoring Centre, Cambridge (UK). <http://data.unep-wcmc.org/datasets/3>.
- Friedlingstein, P., Jones, M.W., O'Sullivan, M., Andrew, R.M., Hauck, J., Peters, G.P., Peters, W., Pongratz, J., Sitch, S., Le Quéré, C., Bakker, D.C.E., Canadell, J.G., Ciais, P., Jackson, R.B., Anthoni, P., Barbero, L., Bastos, A., Bastrikov, V., Becker, M., Bopp, L., Buitenhuis, E., Chandra, N., Chevallier, F., Chini, L.P., Currie, K.I., Feely, R.A., Gehlen, M., Gilfillan, D., Gkritzalis, T., Goll, D.S., Gruber, N., Gutekunst, S., Harris, I., Havard, V., Houghton, R.A., Hurtt, G., Ilyina, T., Jain, A.K., Joetzjer, E., Kaplan, J.O., Kato, E., Goldewijk, K.K., Korsbakken, J.I., Landschützer, P., Lauvset, S.K., Lefevre, N., Lenton, A., Lienert, S., Lombardozi, D., Marland, G., McGuire, P.C., Melton, J.R., Metz, N., Munro, D.R., Nabel, J.E.M.S., Nakaoka, S.-I., Neill, C., Omar, A.M., Ono, T., Peregon, A., Pierrot, D., Poulter, B., Rehder, G., Resplandy, L., Robertson, E., Rödenbeck, C., Séférian, R., Schwinger, J., Smith, N., Tans, P.P., Tian, H., Tilbrook, B., Tubiello, F.N., van der Werf, G.R., Wiltshire, A.J., Zaehle, S., 2019. Global carbon budget 2019. *Earth Syst. Sci. Data* 11, 1783–1838. <https://doi.org/10.5194/essd-11-1783-2019>.
- Friis, K., Körtzinger, A., Wallace, D.W.R., 2003. The salinity normalization of marine inorganic carbon chemistry data. *Geophys. Res. Lett.* 30, 1085. <https://doi.org/10.1029/2002GL015898>.
- Fröb, F., Olsen, A., Våge, K., Moore, G.W.K., Yashayaev, I., Jeansson, E., Rajasakaren, B., 2016. Irminger Sea deep convection injects oxygen and anthropogenic carbon to the ocean interior. *Nat. Commun.* 7, 13244. <https://doi.org/10.1038/ncomms13244>.
- Fröb, F., Olsen, A., Pérez, F.F., García-Ibañez, L.I., Jeansson, E., Omar, A., Lauvset, S.K., 2018. Inorganic carbon and water masses in the Irminger sea since 1991. *Biogeosciences* 15, 51–72. <https://doi.org/10.5194/bg-15-51-2018>.
- García-Ibañez, M.I., Zunino, P., Fröb, F., Carracedo, L.I., Ríos, A.F., Mercier, H., Olsen, A., Pérez, F.F., 2016. Ocean acidification in the subpolar North Atlantic: rates and mechanisms controlling pH changes. *Biogeosciences* 13, 3701–3715. <https://doi.org/10.5194/bg-13-3701-2016>.
- Gattuso, J.P., Brewer, P., Hoegh-Guldberg, O., Kleypas, J.A., Pörtner, H.-O., Schmidt, D., 2014. Ocean acidification. In: Field, C.B., Barros, V.R., Dokken, D.J., Mach, K.J., Mastrandrea, M.D., Bilir, T.E., White, L.L. (Eds.), *Climate Change 2014: Impacts, Adaptation, and Vulnerability. Part A: Global and Sectoral Aspects. Contribution of Working Group II to the Fifth Assessment Report of the Intergovernmental Panel on Climate Change*. Cambridge University Press, Cambridge, United Kingdom and New York, NY, USA, pp. 129–131.
- Gehlen, M., Séférian, R., Jones, D.O.B., Roy, T., Roth, R., Barry, J., Bopp, L., Doney, S.C., Dunne, J.P., Heinze, C., Joos, F., Orr, J.C., Resplandy, L., Segschneider, J., Tjiputra, J., 2014. Projected pH reductions by 2100 might put deep North Atlantic biodiversity at risk. *Biogeosciences* 11, 6955–6967. <https://doi.org/10.5194/bg-11-6955-2014>.
- Gruber, N., Clement, D., Carter, B.R., Feely, R.A., van Heuven, S., Hoppema, M., Ishii, M., Key, R.M., Kozyr, A., Lauvset, S.K., Lo Monaco, C., Mathis, J.T., Murata, A., Olsen, A., Perez, F.F., Sabine, C.L., Tanhua, T., Wanninkhof, R., 2019. The oceanic sink for anthropogenic CO₂ from 1994 to 2007. *Science* 363, 1193–1199. <https://doi.org/10.1126/science.aau5153>.
- Guallart, E.F., Schuster, U., Fajar, N.M., Legge, O., Brown, P., Pelejero, C., Messias, M.-J., Calvo, E., Watson, A., Ríos, A.F., Pérez, F.F., 2015. Trends in anthropogenic CO₂ in water masses of the Subtropical North Atlantic Ocean. *Prog. Oceanogr.* 131, 21–32. <https://doi.org/10.1016/j.poccean.2014.11.006>.
- Guinotte, J.M., Orr, J., Cairns, S., Freiwald, A., Morgan, L., George, R., 2006. Will human-induced changes in seawater chemistry alter the distribution of deep-sea scleractinian corals? *Front. Ecol. Environ.* 4, 141–146. [https://doi.org/10.1890/1540-9295\(2006\)004\[0141:WHCISC\]2.0.CO;2](https://doi.org/10.1890/1540-9295(2006)004[0141:WHCISC]2.0.CO;2).
- Häkkinen, S., Rhines, P.B., 2004. Decline of subpolar North Atlantic circulation during the 1990s. *Science* 304, 555–559. <https://doi.org/10.1126/science.1094917>.
- Hansen, B., Húsgrå Larsen, K.M., Hátún, H., Østerhus, S., 2016. A stable Faroe Bank Channel overflow 1995–2015. *Ocean Sci.* 12, 1205–1220. <https://doi.org/10.5194/os-12-1205-2016>.
- Hauri, C., Gruber, N., Vogt, M., Doney, S.C., Feely, R.A., Lachkar, Z., Leinweber, A., McDonnell, A.M.P., Munnich, M., Plattner, G.-K., 2013. Spatiotemporal variability and long-term trends of ocean acidification in the California Current System. *Biogeosciences* 10, 193–216. <https://doi.org/10.5194/bg-10-193-2013>.
- Hennige, S.J., Wicks, L.C., Kamenos, N.A., Bakker, D.C.E., Findlay, H.S., Dumousseaud, C., Roberts, J.M., 2014. Short-term metabolic and growth responses of the cold-water coral *Lophelia pertusa* to ocean acidification. *Deep Sea Res. Part II Top. Stud. Oceanogr.* 99, 27–35. <https://doi.org/10.1016/j.dsr2.2013.07.005>.
- Hennige, S.J., Wicks, L.C., Kamenos, N.A., Perna, G., Findlay, H.S., Roberts, J.M., 2015. Hidden impacts of ocean acidification to live and dead coral framework. *Proc. R. Soc. B* 282, 20150990. <https://doi.org/10.1098/rspb.2015.0990>.
- Hennige, S.J., Wolfram, U., Wickes, L., Murray, F., Roberts, J.M., Kamenos, N.A., Schofield, S., Groetsch, A., Spiesz, E.M., Aubin-Tam, M.-E., Etnoyer, P.J., 2020. Crumbling reefs and cold-water coral habitat loss in a future ocean: evidence of “Coralporosis” as an indicator of habitat integrity. *Front. Mar. Sci.* 7, 668. <https://doi.org/10.3389/fmars.2020.00668>.
- IPCC, 2011. *Workshop report of the Intergovernmental panel on climate change workshop on impacts of ocean acidification on marine biology and ecosystems*. In: Field, C.B., Barros, V., Stocker, T.F., Qin, D., Mach, K.J., Plattner, G.-K., Ebi, K.L. (Eds.), *IPCC Working Group II Technical Support Unit*. Carnegie Institution, Stanford, California, United States of America, 164 pp.
- Jiang, L.-Q., Feely, R.A., Carter, B.R., Greeley, D.J., Gledhill, D.K., Arzayus, K.M., 2015. Climatological distribution of aragonite saturation state in the global oceans. *Glob. Biogeochem. Cycles* 29, 2015GB005198. <https://doi.org/10.1002/2015GB005198>.
- Jiang, L.Q., Carter, B.R., Feely, R.A., Lauvset, S.K., Olsen, A., 2019. Surface ocean pH and buffer capacity: past, present and future. *Sci. Rep.* 9, 18624. <https://doi.org/10.1038/s41598-019-55039-4>.
- Keeling, C.D., Brix, H., Gruber, N., 2004. Seasonal and long-term dynamics of the upper ocean carbon cycle at Station ALOHA near Hawaii. *Glob. Biogeochem. Cycles* 18, GB4006. <https://doi.org/10.1029/2004GB002227>.

- Key, R.M., Olsen, A., van Heuven, S., Lauvset, S.K., Velo, A., Lin, X., Schirnick, C., Kozyr, A., Tanhua, T., Hoppema, M., Jutterström, S., Steinfeldt, R., Jeansson, E., Ishii, M., Pérez, F.F., Suzuki, T., 2015. Global ocean data analysis project, version 2 (GLODAPv2). In: ORNL/CDIAC-162, NDP-093, Carbon Dioxide Information Analysis Center. Oak Ridge National Laboratory, Oak Ridge, Tennessee, US.
- Khatiwala, S., Tanhua, T., Mikaloff Fletcher, S., Gerber, M., Doney, S.C., Graven, H.D., Gruber, N., McKinley, G.A., Murata, A., Ríos, A.F., Sabine, C.L., 2013. Global Ocean storage of anthropogenic carbon. *Biogeosciences* 10, 2169–2191. <https://doi.org/10.5194/bg-10-2169-2013>.
- Kieke, D., Yashayaev, I., 2015. Studies of Labrador Sea Water formation and variability in the subpolar North Atlantic in the light of international partnership and collaboration. *Prog. Oceanogr.* 132, 220–232. <https://doi.org/10.1016/j.pcean.2014.12.010>.
- Kieke, D., Rhein, M., Stramma, L., Smethie, W.M., LeBel, D.A., Zenk, W., 2006. Changes in the CFC inventories and formation rates of Upper Labrador Sea Water, 1997–2001. *J. Phys. Oceanogr.* 36, 64–86. <https://doi.org/10.1175/JPO2814.1>.
- Kieke, D., Rhein, M., Stramma, L., Smethie, W.M., Bullister, J.L., LeBel, D.A., 2007. Changes in the pool of Labrador Sea Water in the subpolar North Atlantic. *Geophys. Res. Lett.* 34, L06605. <https://doi.org/10.1029/2006GL028959>.
- Kriegler, E., Bauer, N., Popp, A., Humpenöder, F., Leimbach, M., Strefler, J., Baumstark, L., Bodirsky, B.L., Hilaire, J., Klein, D., Mouratiadou, I., Weindl, I., Bertram, C., Dietrich, J.-P., Luderer, G., Pehl, M., Pietzcker, R., Piontek, F., Lotze-Campen, H., Biewald, A., Bonsch, M., Giannousakis, A., Kreidenweis, U., Müller, C., Rolinski, S., Schultes, A., Schwanitz, J., Stevanovic, M., Calvin, K., Emmerling, J., Fujimori, S., Edenhofer, O., 2017. Fossil-fueled development (SSP5): an energy and resource intensive scenario for the 21st century. *Glob. Environ. Chang.* 42, 297–315. <https://doi.org/10.1016/j.gloenvcha.2016.05.015>.
- Kroeker, K.J., Kordas Ryan, R.C., Hendriks, I., Ramajo, L., Singh, G., Duarte, C., Gattuso, J., 2013. Impacts of ocean acidification on marine organisms: quantifying sensitivities and interaction with warming. *Glob. Chang. Biol.* 19 (6), 1884–1896. <https://doi.org/10.1111/gcb.12179>.
- Kwiatkowski, L., Orr, J.C., 2018. Diverging seasonal extremes for ocean acidification during the twenty-first century. *Nat. Clim. Chang.* 8 (2), 141–145. <https://doi.org/10.1038/s41558-017-0054-0>.
- Lazier, J., Hendry, R., Clarke, A., Yashayaev, I., Rhines, P., 2002. Convection and restratification in the Labrador Sea, 1990–2000. *Deep Sea Res. Part I Oceanogr. Res. Pap.* 49, 1819–1835. [https://doi.org/10.1016/S0967-0637\(02\)00064-X](https://doi.org/10.1016/S0967-0637(02)00064-X).
- Leseurre, C., Lo Monaco, C., Reverdin, G., Metzl, N., Fin, J., Olafsdottir, S., Racapé, V., 2020. Ocean carbonate system variability in the North Atlantic Subpolar surface water (1993–2017). *Biogeosciences* 17, 2553–2577. <https://doi.org/10.5194/bg-17-2553-2020>.
- Lewis, E., Wallace, D.W.R., 1998. Program developed for CO₂ System Calculations. In: ORNL/CDIAC-105. Dioxide Information Analysis Center, Oak Ridge National Laboratory, US Department of Energy, Oak Ridge, TN, Carbon.
- Lherminier, P., 2018. OVIDE 2018 cruise. RV Thalassa. <https://doi.org/10.17600/18000510>.
- Lovenduski, N.S., Gruber, N., Doney, S.C., Lima, I.D., 2007. Enhanced CO₂ outgassing in the Southern Ocean from a positive phase of the Southern Annular Mode. *Glob. Biogeochem. Cycles* 21, GB2026. <https://doi.org/10.1029/2006GB002900>.
- Lueker, T.J., Dickson, A.G., Keeling, C.D., 2000. Ocean pCO₂ calculated from dissolved inorganic carbon, alkalinity, and equations for K₁ and K₂: validation based on laboratory measurements of CO₂ in gas and seawater at equilibrium. *Mar. Chem.* 70, 105–119. [https://doi.org/10.1016/S0304-4203\(00\)00022-0](https://doi.org/10.1016/S0304-4203(00)00022-0).
- Maier, C., Hegeman, J., Weinbauer, M.G., Gattuso, J.-P., 2009. Calcification of the cold-water coral *Lophelia pertusa*, under ambient and reduced pH. *Biogeosciences* 6, 1671–1680. <https://doi.org/10.5194/bg-6-1671-2009>.
- Matear, R.J., Lenton, A., 2014. Quantifying the impact of ocean acidification on our future climate. *Biogeosciences* 11, 3965–3983. <https://doi.org/10.5194/bg-11-3965-2014>.
- Mehrbach, C., Culbertson, C.H., Hawley, J.E., Pytkowicz, R.M., 1973. Measurement of the apparent dissociation constants of carbonic acid in seawater at atmospheric pressure. *Limnol. Oceanogr.* 18, 897–907. <https://doi.org/10.4319/lo.1973.18.6.0897>.
- Millero, F.J., 1995. Thermodynamics of the carbon dioxide system in the oceans. *Geochim. Cosmochim. Acta* 59, 661–677. [https://doi.org/10.1016/0016-7037\(94\)00354-0](https://doi.org/10.1016/0016-7037(94)00354-0).
- Millero, F.J., Feistel, R., Wright, D.G., McDougall, T.J., 2008. The composition of standard seawater and the definition of the reference-composition salinity scale. *Deep-Sea Res. Pt. I* 55, 50–72. <https://doi.org/10.1016/j.dsr.2007.10.001>.
- Milliman, J.D., Troy, P.J., Balch, W.M., Adams, A.K., Li, Y.-H., Mackenzie, F.T., 1999. Biologically mediated dissolution of calcium carbonate above the chemical lysocline? *Deep Sea Res. Part I Oceanogr. Res. Pap.* 46, 1653–1669. [https://doi.org/10.1016/S0967-0637\(99\)00034-5](https://doi.org/10.1016/S0967-0637(99)00034-5).
- Mostafa, K.M., Liu, C., Zhai, W., Minella, M., Vione, D., Gao, K., Minakata, D., Arakaki, T., Yoshioka, T., Hayakawa, K., Konohira, E., Tanoue, E., Akhand, A., Chanda, A., Wang, B., Sakugawa, H., 2016. Reviews and Syntheses: Ocean acidification and its potential impacts on marine ecosystems. *Biogeosciences* 13, 1767–1786. <https://doi.org/10.5194/bg-13-1767-2016>.
- Mucci, A., 1983. The solubility of calcite and aragonite in seawater at various salinities, temperatures, and one atmosphere total pressure. *Am. J. Sci.* 283, 780–799. <https://doi.org/10.2475/ajs.283.7.780>.
- Murata, A., Hayashi, K., Kumamoto, Y., Sasaki, K., 2015. Detecting the progression of ocean acidification from the saturation state of CaCO₃ in the subtropical South Pacific. *Glob. Biogeochem. Cycles* 29, 463–475. <https://doi.org/10.1002/2014GB004908>.
- Olafsson, J., Olafsdottir, S.R., Benoit-Cattin, A., Danielsen, M., Arnarson, T.S., Takahashi, T., 2009. Rate of Iceland Sea acidification from time series measurements. *Biogeosciences* 6, 2661–2668. <https://doi.org/10.5194/bg-6-2661-2009>.
- Olsen, A., Lange, N., Key, R.M., Tanhua, T., Bittig, H.C., Kozyr, A., Álvarez, M., Azetsu-Scott, K., Becker, S., Brown, P.J., Carter, B.R., Cotrim da Cunha, L., Feely, R.A., van Heuven, S., Hoppema, M., Ishii, M., Jeansson, E., Jutterström, S., Landa, C.S., Lauvset, S.K., Michaelis, P., Murata, A., Pérez, F.F., Pfeil, B., Schirnick, C., Steinfeldt, R., Suzuki, T., Tilbrook, B., Velo, A., Wanninkhof, R., Woosley, R.J., 2020. An updated version of the global interior ocean biogeochemical data product, GLODAPv2.2020. *Earth Syst. Sci. Data* 12, 3653–3678. <https://doi.org/10.5194/essd-12-3653-2020>.
- Omar, A.M., Skjelvan, I., Erga, S.R., Olsen, A., 2016. Aragonite saturation states and pH in western Norwegian fjords: seasonal cycles and controlling factors, 2005–2009. *Ocean Sci.* 12, 937–951. <https://doi.org/10.5194/os-12-937-2016>.
- Orr, J.C., Fabry, V.J., Aumont, O., Bopp, L., Doney, S.C., Feely, R.A., Gnanadesikan, A., Gruber, N., Ishida, A., Joos, F., Key, R.M., Lindsay, K., Maier-Reimer, E., Matear, R., Monfray, P., Mouchet, A., Najjar, R.G., Plattner, G.-K., Rodgers, K.B., Sabine, C.L., Sarmiento, J.L., Schlitzer, R., Slater, R.D., Totterdell, I.J., Weirig, M.F., Yamanaka, Y., Yool, A., 2005. Anthropogenic Ocean acidification over the twenty-first century and its impact on calcifying organisms. *Nature* 437, 681–686. <https://doi.org/10.1038/nature04095>.
- Orr, J.C., Epitalon, J.-M., Dickson, A.G., Gattuso, J.-P., 2018. Routine uncertainty propagation for the marine carbon dioxide system. *Mar. Chem.* 207, 84–107. <https://doi.org/10.1016/j.marchem.2018.10.006>.
- Pérez, F.F., Vázquez-Rodríguez, M., Louarn, E., Padín, X.A., Mercier, H., Ríos, A.F., 2008. Temporal variability of the anthropogenic CO₂ storage in the Irminger Sea. *Biogeosciences* 5, 1669–1679. <https://doi.org/10.5194/bg-5-1669-2008>.
- Pérez, F.F., Mercier, H., Vázquez-Rodríguez, M., Lherminier, P., Velo, A., Pardo, P.C., Rosón, G., Ríos, A.F., 2013. Atlantic Ocean CO₂ uptake reduced by weakening of the meridional overturning circulation. *Nat. Geosci.* 6, 146–152. <https://doi.org/10.1038/ngeo1680>.
- Pérez, F.F., Fontela, M., García-Ibáñez, M.I., Lherminier, P., Zunino, P., de la Paz, M., Padín, X.A., Alonso-Pérez, F., Velo, A., Gualart, E.F., Mercier, H., 2018. Meridional overturning circulation conveys fast acidification to the deep Atlantic Ocean. *Nature* 554, 515–518. <https://doi.org/10.1038/nature25493>.
- Pörtner, H.-O., Karl, D.M., Boyd, P.W., Cheung, W.W.L., Lluich-Cota, S.E., Nojiri, Y., Schmidt, D.N., Zavalov, P.O., 2014. Ocean systems. In: Field, C.B., Barros, V.R., Dokken, D.J., Mach, K.J., Mastrandrea, M.D., Bilir, T.E., White, L.L. (Eds.), *Climate Change 2014: Impacts, Adaptation, and Vulnerability. Part A: Global and Sectoral Aspects. Contribution of Working Group II to the Fifth Assessment Report of the Intergovernmental Panel on Climate Change*. Cambridge University Press, Cambridge, United Kingdom and New York, NY, USA, pp. 411–484.
- Ragazzola, F., Foster, L.C., Form, A., Anderson, P.S.L., Hansteen, T.H., Fietzke, J., 2012. Ocean acidification weakens the structural integrity of coralline algae. *Glob. Chang. Biol.* 18 (9), 2804–2812. <https://doi.org/10.1111/j.1365-2486.2012.02756.x>.
- Raven, J., Caldeira, K., Elderfield, H., Hoegh-Guldberg, O., Liss, P., Riebesell, U., Shepherd, J., Turley, C., Watson, A., 2005. Ocean acidification due to increasing atmospheric carbon dioxide. *R. Soc. Lond. Document No. 12/05*, 68 pages.
- Rhein, M., Kieke, D., Steinfeldt, R., 2007. Ventilation of the Upper Labrador Sea Water, 2003–2005. *Geophys. Res. Lett.* 34, L06603. <https://doi.org/10.1029/2006GL028540>.
- Riahi, K., van Vuuren, D.P., Kriegler, E., Edmonds, J., O'Neill, B.C., Fujimori, S., Bauer, N., Calvin, K., Dellink, R., Fricko, O., Lutz, W., Popp, A., Crespo Cuaresma, J., KC, S., Leimbach, M., Jiang, L., Kram, T., Rao, S., Emmerling, J., Ebi, K., Hasegawa, T., Havlik, P., Humpenöder, F., Aleluia Da Silva, L., Smith, S., Stehfest, E., Bosetti, V., Eom, J., Gernaat, D., Masui, T., Rogelj, J., Strefler, J., Drouet, L., Krey, V., Luderer, G., Harmsen, M., Takahashi, K., Baumstark, L., Doelman, J.C., Kainuma, M., Klimont, Z., Marangoni, G., Lotze-Campen, H., Obersteiner, M., Tabeau, A., Tavoni, M., 2017. The shared socioeconomic pathways and their energy, land use, and greenhouse gas emissions implications: An overview. *Global Environmental Change* 42, 153–168. <https://doi.org/10.1016/j.gloenvcha.2016.05.009>.
- Riebesell, U., Zondervan, I., Rost, B., Tortell, P.D., Zeebe, R.E., Morel, F.M.M., 2000. Reduced calcification of marine plankton in response to increased atmospheric CO₂. *Nature* 407, 364–367. <https://doi.org/10.1038/35030078>.
- Riley, J.P., Tongudai, M., 1967. The major cation/chlorinity ratios in sea water. *Chem. Geol.* 2, 263–269. [https://doi.org/10.1016/0009-2541\(67\)90026-5](https://doi.org/10.1016/0009-2541(67)90026-5).
- Ríos, A., Pardo, P.C., Hoppema, M., Pérez, F.F., 2012. An update of anthropogenic CO₂ storage rates in the western South Atlantic basin and the role of Antarctic Bottom Water. *J. Mar. Syst.* 94, 197–203. <https://doi.org/10.1016/j.jmarsys.2011.11.023>.
- Roberts, J.M., Wheeler, A.J., Freiwald, A., Cairns, S., 2009. *Cold-Water Corals: The Biology and Geology of Deep-Sea Coral Habitats*. Cambridge University Press, Cambridge. <https://doi.org/10.1017/CBO9780511581588>.
- Sabine, C.L., Feely, R.A., Gruber, N., Key, R.M., Lee, K., Bullister, J.L., Wanninkhof, R., Wong, C.S., Wallace, D.W.R., Tilbrook, B., Millero, F.J., Peng, T.-H., Kozyr, A., Ono, T., Ríos, A.F., 2004. The Oceanic Sink for Anthropogenic CO₂. *Science* 305, 367–371. <https://doi.org/10.1126/science.1097403>.
- Sanford, T., Frumhoff, P.C., Luers, A., Gullede, J., 2014. The climate policy narrative for a dangerously warming world. *Natural Climate Change* 4, 164–166. <https://doi.org/10.1038/nclimate2148>.
- Sarafanov, A., Mercier, H., Falina, A., Sokov, A., Lherminier, P., 2010. Cessation and partial reversal of deep water freshening in the northern North Atlantic: observation-based estimates and attribution. *Tellus A* 62, 80–90. <https://doi.org/10.1111/j.1600-0870.2009.00418.x>.
- Sarmiento, J.L., Le Qué, C., Pacala, S.W., 1995. Limiting future atmospheric carbon dioxide. *Global Biogeochem. Cycles* 9 (1), 121–137. <https://doi.org/10.1029/94GB01779>.
- Schlitzer, R., 2020. Ocean Data View. <http://odv.awi.de>.

- Takahashi, T., Sutherland, S.C., Chipman, D.W., Goddard, J.G., Ho, C., Newberger, T., Sweeney, C., Munro, D.R., 2014. Climatological distributions of pH, b, total CO₂, alkalinity, and CaCO₃ saturation in the global surface ocean, and temporal changes at selected locations. *Mar. Chem.* 164, 95–125. <https://doi.org/10.1016/j.marchem.2014.06.004>.
- Tanhua, T., Körtzinger, A., Friis, K., Waugh, D.W., Wallace, D.W., 2007. An estimate of anthropogenic CO₂ inventory from decadal changes in oceanic carbon content. *Proc. Natl. Acad. Sci.* 104, 3037–3042. <https://doi.org/10.1073/pnas.0606574104>.
- Thierry, V., de Boissésion, E., Mercier, H., 2008. Interannual variability of the Subpolar Mode Water properties over the Reykjanes Ridge during 1990–2006. *J. Geophys. Res. Oceans* 113, C04016. <https://doi.org/10.1029/2007JC004443>.
- Thresher, R.E., Tilbrook, B., Fallon, S., Wilson, N.C., Adkins, J., 2011. Effects of chronic low carbonate saturation levels on the distribution, growth and skeletal chemistry of deep-sea corals and other seamount megabenthos. *Mar. Ecol. Prog. Ser.* 442, 87–99. <https://doi.org/10.3354/meps09400>.
- Tittensor, D.P., Baco, A.R., Hall-Spencer, J.M., Orr, J.C., Rogers, A.D., 2010. Seamounts as refugia from ocean acidification for cold-water stony corals. *Mar. Ecol.* 31, 212–225. <https://doi.org/10.1111/j.1439-0485.2010.00393.x>.
- Turi, G., Lachkar, Z., Gruber, N., Münnich, M., 2016. Climatic modulation of recent trends in ocean acidification in the California Current System. *Environ. Res. Lett.* 11, 014007. <https://doi.org/10.1088/1748-9326/11/1/014007>.
- Turley, C.M., Roberts, J.M., Guinotte, J.M., 2007. Corals in deep-water: will the unseen hand of ocean acidification destroy cold-water ecosystems? *Coral Reefs* 26, 445–448. <https://doi.org/10.1007/s00338-007-0247-5>.
- Uppström, L.R., 1974. Boron/chlorinity ratio of deep-sea water from the Pacific Ocean. *Deep-Sea Res.* 21, 161–162. [https://doi.org/10.1016/0011-7471\(74\)90074-6](https://doi.org/10.1016/0011-7471(74)90074-6).
- Våge, K., Pickart, R.S., Thierry, V., Reverdin, G., Lee, C.M., Petrie, B., Agnew, T.A., Wong, A., Ribergaard, M.H., 2009. Deep convection returns to the subpolar North Atlantic. *Nat. Geosci.* 2 (1), 67–72. <https://doi.org/10.1038/ngeo382>.
- van Aken, H.M., 2000. The hydrography of the mid-latitude Northeast Atlantic Ocean: I: the deep water masses. *Deep Sea Res. Part I Oceanogr. Res. Pap.* 47, 757–788. [https://doi.org/10.1016/S0967-0637\(99\)00092-8](https://doi.org/10.1016/S0967-0637(99)00092-8).
- van Heuven, S., Pierrot, D., Lewis, E., Wallace, D., 2011. MATLAB Program developed for CO₂ System Calculations. In: ORNL/CDIAC-105b, Carbon Dioxide Information Analysis Center, Oak Ridge National Laboratory. US Department of Energy, Oak Ridge, TN.
- Vázquez-Rodríguez, M., Touratier, F., Lo Monaco, C., Waugh, D.W., Padin, X.A., Bellerby, R.G.J., Goyet, C., Metzl, N., Ríos, A.F., Pérez, F.F., 2009. Anthropogenic carbon distributions in the Atlantic Ocean: data-based estimates from the Arctic to the Antarctic. *Biogeosciences* 6, 439–451. <https://doi.org/10.5194/bg-6-439-2009>.
- Vázquez-Rodríguez, M., Pérez, F.F., Velo, A., Ríos, A.F., Mercier, H., 2012. Observed acidification trends in the North Atlantic water masses. *Biogeosciences* (9), 5217–5230. <https://doi.org/10.5194/bg-9-5217-2012>.
- Velo, A., Pérez, F.F., Tanhua, T., Gilcoto, M., Ríos, A.F., Key, R.M., 2013. Total alkalinity estimation using MLR and neural network techniques. *J. Mar. Syst.* 111–112, 11–18. <https://doi.org/10.1016/j.jmarsys.2012.09.002>.
- Wallace, W.R., 2001. Storage and transport of excess CO₂ in the oceans: The JGOFS/WOCE global CO₂ survey. In: Church, J., Gould, J. (Eds.), *Siedler, G. Academic Press, Ocean Circulation and Climate*, pp. 489–521.
- Williams, N.L., Feely, R.A., Sabine, C.L., Dickson, A.G., Swift, J.H., Talley, L.D., Russell, J.L., 2015. Quantifying anthropogenic carbon inventory changes in the Pacific sector of the Southern Ocean. *Mar. Chem.* 174, 147–160. <https://doi.org/10.1016/j.marchem.2015.06.015>.
- Williamson, P., Widdicombe, S., 2018. The rise of CO₂ and ocean acidification. In: Elias, S., Alderton, D.H.M., Bliznak, V., Cochran, J.K., Dellasala, D.A., Funicello, F., Yang, X.J. (Eds.), *Reference Module in Earth Systems and Environmental Sciences*, from Encyclopedia of the Anthropocene, Volume 5. Elsevier, Oxford, pp. 51–59. <https://doi.org/10.1016/B978-0-12-809665-9.09877-3>.
- Xu, Y.Y., Cai, W.J., Wanninkhof, R., Salisbury, J., Reimer, J., Chen, B., 2020. Long-term changes of carbonate chemistry variables along the north american east coast. *J. Geophys. Res. Oceans* 125, e2019JC015982. <https://doi.org/10.1029/2019JC015982>.
- Xue, L., Yang, X., Li, Y., Li, L., Jiang, L.-Q., Xin, M., Wang, Z., Sun, X., Wei, Q., 2020. Processes controlling sea surface pH and aragonite saturation state in a large northern temperate bay: Contrasting temperature effects. *J. Geophys. Res.: Biogeosci.* 125, e2020JG005805. <https://doi.org/10.1029/2020JG005805>.
- Yashayaev, I., 2007. Hydrographic changes in the Labrador Sea, 1960–2005. *Prog. Oceanogr.* 73, 242–276. <https://doi.org/10.1016/j.pocean.2007.04.015>.
- Yashayaev, I., Dickson, R., 2008. Transformation and fate of overflows in the Northern North Atlantic. In: Dickson, R.R., Meincke, J., Rhines, P. (Eds.), *Arctic-Subarctic Ocean Fluxes: defining the Role of the Northern Seas in climate*. Springer Netherlands, pp. 569–612.
- Yashayaev, I., Loder, J.W., 2009. Enhanced production of labrador sea water in 2008. *Geophys. Res. Lett.* 36, L01606. <https://doi.org/10.1029/2008GL036162>.
- Yashayaev, I., Loder, J.W., 2016. Recurrent replenishment of Labrador Sea Water and associated decadal-scale variability. *J. Geophys. Res. Oceans* 121, 8095–8114. <https://doi.org/10.1002/2016JC012046>.
- Yashayaev, I., Holliday, N.P., Bersch, M., van Aken, H.M., 2008. The history of the Labrador Sea water: production, spreading, transformation and loss. In: Dickson, R. R., Meincke, J., Rhines, P. (Eds.), *Arctic-Subarctic Ocean Fluxes: defining the Role of the Northern Seas in climate*. Springer Netherlands, pp. 569–612.
- Zeebe, R.E., Wolf-Gladrow, D.A., 2001. CO₂ in seawater: equilibrium, kinetics, isotopes. *Elsevier Oceanography Series* 65, 360 pp.